Thanatin targets the intermembrane protein complex required for lipopolysaccharide transport in Escherichia coli

Vetterli, Stefan U ; Zerbe, Katja ; Müller, Maik ; Urfer, Matthias ; Mondal, Milon ; Wang, Shuang-Yan ; Moehle, Kerstin ; Zerbe, Oliver ; Vitale, Alessandra ; Pessi, Gabriella ; Eberl, Leo ; Wollscheid, Bernd ; Robinson, John A

Abstract: With the increasing resistance of many Gram-negative bacteria to existing classes of antibiotics, identifying new paradigms in antimicrobial discovery is an important research priority. Of special interest are the proteins required for the biogenesis of the asymmetric Gram-negative bacterial outer membrane (OM). Seven Lpt proteins (LptA-G) associate in most Gram-negative bacteria to form a macromolecular complex spanning the entire envelope, which transports lipopolysaccharide (LPS) molecules from their site of assembly at the inner membrane to the cell surface, powered by adenosine 5 -triphosphate hydrolysis in the cytoplasm. The periplasmic protein LptA comprises the protein bridge across the periplasm, which connects LptB2FGC at the inner membrane to LptD/E anchored in the OM. We show here that the naturally occurring, insect-derived antimicrobial peptide thanatin targets LptA and LptD in the network of periplasmic protein-protein interactions required to assemble the Lpt complex, leading to the inhibition of LPS transport and OM biogenesis in Escherichia coli.

DOI: https://doi.org/10.1126/sciadv.aau2634

Thanatin Targets the Inter-Membrane Protein Complex Required for Lipopolysaccharide Transport in *Escherichia coli*

Stefan U. Vetterli[1], Katja Zerbe[1], Maik Mueller[3], Matthias Urfer[1], Milon Mondal[1], Shuang-Yan Wang[1], Kerstin Moehle[1], Oliver Zerbe[1], Alessandra Vitale[2], Gabriella Pessi[2], Leo Eberl[2], Bernd Wollscheid[3] & John A. Robinson*[1]

[1] Chemistry Department, University of Zurich, Winterthurerstrasse 190, 8057 Zurich, Switzerland.

[2] Department of Plant and Microbial Biology, University of Zurich, Zollikerstrasse 107, 8008 Zurich, Switzerland.

[3] Institute of Molecular Systems Biology & Department of Health Sciences and Technology, ETH Zürich, Auguste-Piccard-Hof 1, 8093 Zürich, Switzerland.

* Correspondence should be addressed to: Chemistry Department, University of Zurich, 8057 Zurich, Switzerland, Tel.: 41-44-635-4242; E-mail: john.robinson@chem.uzh.ch

One sentence summary: Thanatin targets protein-protein interactions between LptA and LptD in the periplasmic bridge required for LPS transport.

Abstract

With the increasing resistance of many Gram-negative bacteria to existing classes of antibiotics, identifying new paradigms in antimicrobial discovery is an important research priority. Of special interest here are the proteins required for the biogenesis of the asymmetric Gram-negative bacterial outer membrane. Seven Lpt proteins (LptA-G) associate in most Gram-negative bacteria to form a macromolecular complex spanning the entire envelope, which transports LPS molecules from their site of assembly at the inner membrane to the cell surface, powered by ATP hydrolysis in the cytoplasm. The periplasmic protein LptA comprises the protein bridge across the periplasm, which connects $LptB_2FGC$ at the inner membrane to LptD/E anchored in the outer membrane. We show here that the naturally occurring insect-derived antimicrobial peptide thanatin targets LptA and LptD in the network of periplasmic protein-protein interactions required to assemble the Lpt complex, leading to inhibition of LPS transport and OM biogenesis in *Escherichia coli*.

Main text

The asymmetric outer membrane (OM) plays a critical role in protecting Gram-negative bacteria from extracellular cytotoxic molecules, including antibiotics. This unique bilayer comprises lipopolysaccharide (LPS) molecules in the outer leaflet and membrane glycerophospholipids in the inner leaflet. Integral OM proteins (OMPs) are crucial for the biogenesis of the OM, as well as for controlling the uptake and export of essential nutrients and signalling molecules across the OM. Of special interest here are the seven proteins (LptA-G) needed to transport LPS molecules from their site of assembly at the inner membrane (IM), across the aqueous periplasm, to their final cell surface location, during OM biogenesis (*1-3*). The LptA-G proteins associate to form a macromolecular complex, which spans the entire envelope (*4, 5*). The periplasmic protein LptA, likely as a head-to-tail oligomer, forms a protein bridge spanning the periplasm. LPS molecules are pushed across this bridge (*6-10*), from $LptB_2FGC$ anchored in the inner membrane, to the LptDE complex embedded in the OM (Figure 1A) (*11, 12 , 13-16*), powered by ATP hydrolysis in the cytoplasm (*4*). We report here that the naturally occurring, insect-derived host-defense peptide thanatin (Figure 1B) targets both LptA and LptD in *Escherichia coli*.

Thanatin was first isolated from the hemipteran insect *Podisus maculiventris* (spined soldier bug) in 1996 (*17*). The peptide contains 21 amino acids (GSKKPVPIIYCNRRTGKCQRM) with a disulfide bond between Cys11 and Cys18. Antimicrobial activity for thanatin was reported against *E. coli*, *Salmonella typhimurium*, *Klebsiella pneumoniae*, and *Enterobacter cloacae* with MICs <1.5 µM, with weaker activity against *Erwinia carotovora* and *Pseudomonas aeruginosa* (MICs 10-12 µM). Whereas no activity was seen against *Staphylococcus aureus*, thanatin is active against several other Gram-positive bacteria with MICs ≈1-5 µM. Of special interest is the observation that the enantiomeric form (D-thanatin) loses much of its activity against all the Gram-negative strains tested, indicating a likely chiral target.

The mechanism of action of thanatin is so far unknown. The peptide is bactericidal against *E. coli*, shows only weak permeabilizing effects on the inner or outer membrane, and

does not cause hemolysis of blood erythrocytes even at 100x the minimal inhibitory concentration (MIC) (*17-20*). We confirmed that thanatin has no membrane-permeabilizing effects on *E. coli*. The fluorescent dye Sytox-Green® does not penetrate *E. coli* cells treated with thanatin even at 100 µg/mL (see section-3, Supplementary Information (SI)). Moreover, no release into the external medium of ß-lactamase expressed in the periplasm, or of ß-galactosidase expressed in the cytoplasm of *E. coli* could be detected upon exposure to thanatin (see SI). Thus, even at concentrations much higher than the minimal inhibitory concentration (MIC), neither the IM nor the OM of *E. coli* are permeabilized by treatment with thanatin, unlike what is seen with some other cationic antimicrobial peptides, such as polymyxin B, colistin or protegrin I (*21, 22*).

The effects of thanatin on macromolecule biosynthesis were examined by monitoring the incorporation of appropriate [^{3}H]-labeled precursors into macromolecules in *E. coli* ATCC25922 (see Section-4, SI). No inhibition of protein, RNA, DNA or cell wall biosynthesis was observed. To analyze effects on morphology, *E. coli* cells were grown with thanatin at concentrations causing significant growth inhibition and then examined in thin sections by transmission electron microscopy (TEM). This revealed frequent defects in membrane architecture, with accumulations of membrane-like material inside cells (Figure 2A/B). Such multilayered membrane folds inside the cell are typical of those reported for *E. coli* in which LPS transport is inhibited by down-regulation of LptA/B, LptC or LptD (*5, 16*). The effects of thanatin on *E. coli* were also monitored by laser scanning stimulated emission depletion (STED) fluorescence microscopy, with staining of membranes by the membrane dye FM4-64, of nucleoids by DAPI, and using Sytox-Green® to detect permeabilized cells (Figure 2C/D). These studies revealed frequent accumulations of membrane-like material in the form of knobs stained bright red by FM4-64, as well as elongated cell assemblies, with neither effect visible in the absence of thanatin. Nucleoids stained with DAPI were not influenced significantly by thanatin, and again no significant staining was observed by Sytox-Green®. These results reveal that thanatin causes defects in membrane assembly in *E. coli*.

A fluorescent derivative (thanatin-BDP-FL; MIC ≈ 1-2 µg/mL, Figure 1B) was used for STED fluorescence imaging. This probe stained the *E. coli* envelope, with marked focal accumulations (as green fluorescent knobs) across the cell and at the cell poles (Figure 2E). This behavior is reminiscent of fluorescent labeling of OM proteins that accumulate into membrane islands or clusters and at the poles in Gram-negative bacteria (*23, 24*). The interaction of thanatin with OM proteins in *E. coli* was tested directly by photoaffinity labeling experiments. Two thanatin-derived photoprobes were synthesized containing photoproline (*25, 26*), in place of either Pro5 or Pro7, together with an N-terminal PEG-linker and biotin tag for pull-down assays (Figure 1B; sections-2 and -6, SI). Both probes (thanatin-PAL5, and thanatin-PAL7) maintained antimicrobial activity against *E. coli* ATCCC25922 (MICs 2-4 µg/mL) and photolabeled the same membrane proteins *in vivo*, as shown in Western blotting for thanatin-PAL5 in Figure 3A. In a competitive photolabeling experiment with native thanatin (200 µg/mL) as competitor, thanatin-PAL5 (2 µg/mL) labeling of the ≈95 kDa band largely disappeared from the blot whereas the other signals showed reduced labeling (Figure 3A). When the in-vivo photolabeled membrane protein extract was analyzed under non-reducing conditions to retain disulfide bonds, a shift of the ≈95 kDa band to ≈130 kDa was seen in the Western blot (Figure 3B, and SI). This change in gel electrophoretic mobility is very characteristic of that reported for *E. coli* LptD in the disulfide-reduced and disulfide-oxidized forms ($LptD_{ox}$ ≈130 kDa; $LptD_{red}$ ≈ 90 kDa) (*27, 28*).

It was technically not possible to identify photolabeled proteins directly from the Western blots. To identify thanatin interaction partners in a hypothesis-free, discovery-driven approach, we used the photoaffinity interaction mapping strategy outlined above, in combination with mass spectrometry-based proteomic analysis, which allows for the multiplexed and label-free quantification of *E. coli* interaction partners. Thanatin-PAL5 photo-labeled and untreated control *E. coli* ATCC25922 cells were lysed and biotinylated proteins purified using streptavidin-functionalized agarose resin. Enriched proteins were proteolytically digested and subsequently identified using high-performance liquid chromatography tandem mass spectrometry (HPLC-MS/MS). Four hundred proteins were

identified at a False-Discovery-Rate (FDR) below 1%. Relative quantitative comparison revealed the specific and photolabeling-dependent enrichment of three proteins, namely LptD, LptA and BamB, of which LptD and LptA were most significant (Figure 3C). Whereas photolabeling of the membrane protein LptD was already suggested by the Western blotting experiments described above, photolabeling of LptA, a small (≈18 kDa) soluble periplasmic component of the LPS transport pathway (Figure 1A), was unexpected.

Spontaneous thanatin resistant (Than^R) mutants of *E. coli* ATCC25922 were sought for genetic analysis. Than^R mutants could be isolated at low frequency (≈ 1 in 10^8 CFUs; 10^{-6} %) by passaging on MH-II agar containing 10-50 µg/mL thanatin. Five Than^R mutants were selected that remained stable over at least four passages on thanatin-free agar (see section-7, SI). Three mutants showed no difference in growth behavior compared to the wild type (wt) in MH-II media and showed no increased sensitivity on MH-II agar supplemented with 0.5% SDS and 1mM EDTA. Also, the susceptibility of all mutants to a series of standard antibiotics was unchanged (see section-7, SI). Whole genome sequencing of the three Than^R mutants revealed several mutations compared to the wt genome, including in *lptA* as the only mutated gene common to all three. Moreover, one resistant mutant (Than^R-8) contained only a single point mutation in the entire genome, corresponding to a change of glutamine to leucine at position 62 (Q62L) in LptA. We also tested whether the identified mutations Q62L-LptA and D31N-LptA would confer resistance to thanatin when introduced into a sensitive *E. coli* strain. For this, genes encoding LptA with a His_6 tag at the C-terminus (LptA-His_6), as well the corresponding mutated variants (Q62L-LptA-His_6, and D31N-LptA-His_6), were introduced into *E. coli*. Introduction of the mutant alleles led to a markedly higher MIC for thanatin, whereas introduction of the wt sequence (LptA-His_6) gave no significant change in MIC (see section-7, SI). In summary, the genetic and photolabeling results reveal a link between the antimicrobial activity of thanatin and LptA, and point to LptA as an interaction partner for thanatin in *E. coli*. On the other hand, no mutations in *lptD* were detected in the genomes of the three analysed Than^R mutants.

To date no small molecules (apart from LPS) are known to interact with LptA, so we tested whether thanatin can directly bind to LptA *in vitro*. A recombinant full-length LptA (with a His_6 tag fused to the C-terminus (LptA-His_6) was produced in *E. coli* BL21(DE3) and purified to apparent homogeneity by SDS-PAGE after Ni-NTA affinity and anion exchange chromatography (see section-8, SI). The binding of thanatin-BDP-FL (Figure 1B) to LptA-His_6 was then studied by fluorescence polarization (FP), and of thanatin binding to LptA labeled with Dylight650 by thermophoresis. Using both biophysical methods, fitting the binding isotherm to a 1:1 Langmuir binding model (see section-9, SI) gave by FP a K_d of 12±3 nM and by thermophoresis of 20±1 nM. In control experiments using the enantiomeric form of thanatin (comprising all D-amino acids), no interaction of D-thanatin with LptA was observed by FP. The binding of thanatin to LptD was also measured *in vitro* using a recombinant His-tagged LptD/E complex purified from *E. coli* (see section-8.2, SI). Using FP, thanatin-BDP-FL binds to $LptD/E_{His}$ with a K_d of 34±5 nM, whereas thermophoresis binding assays gave a K_d of 44±27 nM (see section-10, SI). Thanatin therefore binds *in vitro* to both LptA and LptD/E in the low nanomolar range.

In order to characterize the epitope on LptA involved in binding to thanatin, complex formation was monitored by [^{15}N, ^{1}H]-HSQC NMR spectroscopy, using a recently described, non-aggregating, truncated derivative of LptA called $LptA_m$, lacking the last C-terminal ß-strand (*10*). We confirmed *in vitro* that thanatin binds with the same high affinity also to $LptA_m$ (see section-9, SI). Therefore, the lack of the last C-terminal ß-strand in this $LptA_m$ construct, which is important to prevent unwanted aggregation, does not affect binding to thanatin. This result is understandable, as we show later that thanatin interacts with the N-terminal ß-strands of LptA (*vide infra*). [^{15}N, ^{1}H]-HSQC spectra revealed complete and stable complex formation in the slow exchange regime on the NMR time scale upon addition of thanatin to [^{15}N]-$LptA_m$ to ca. 1:1.2 molar ratio (see section-11, SI). Free $LptA_m$ and the complex of $LptA_m$ with thanatin displayed a high-quality [^{15}N,^{1}H]-HSQC spectrum with good signal dispersion, indicating that the protein-peptide complex was well folded and probably rich in β-sheet. While many ^{1}H-^{15}N correlations in [^{15}N]-$LptA_m$ were unchanged upon thanatin

binding, a multitude of other cross-peaks showed significant chemical shift perturbations (CSPs, see section-11, SI). The structure of the thanatin-LptA$_m$ complex (Figure 4A) was then determined by multidimensional NMR methods using mixtures of unlabeled and [^{13}C,^{15}N]-labeled forms of thanatin and LptA$_m$ in isotope-edited/filtered NOESY experiments.

In the complex, the N-terminal strand of the thanatin ß-hairpin (Pro^{7}-Asn^{12}) docks in a parallel orientation onto the first ß-strand in the ß-jellyroll of LptA$_m$ (Pro^{35}-Ser^{40}), with the strand orientation being clearly defined by multiple interstrand NOEs (Figure 4B). Following the ß-turn in thanatin (Arg^{13}-Gly^{16}), the C-terminal strand (Lys^{17}-Met^{21}) is mostly solvent exposed (Figure 4A,C), although the side-chain of Met^{21} nestles into a hydrophobic site on the surface of LptA$_m$. Hydrophobic residues on the thanatin N-terminal ß-strand, in particular Ile^{8} and Tyr^{10}, are buried in the hydrophobic interior of the ß-jellyroll (Figure 4A), in a cavity formed by LptA$_m$ side chains Ile^{38}, Leu^{45}, Val^{52}, Phe^{54}, Val^{74}, Ile^{86}, as evidenced by a network of NOEs seen in NOESY spectra. It seems likely that multiple van der Waals contacts and a pi-pi stacking interaction (Than.Tyr^{10}-LptA$_m$.Phe^{54}) made between these residues may help to stabilize the complex. Moreover, aliphatic residues of thanatin (Val^{6}, Pro^{7}) pack against Pro^{35} and Ile^{36} near to the N-terminus of LptA$_m$ thereby forming another hydrophobic interaction, which helps to establish the orientation of the N-terminal part of thanatin. This interaction affects the orientation of the short N-terminal helix in LptA$_m$ including Asp^{31}, which in turn packs against a loop of the ß-jellyroll containing Gln^{62} (Figure 4C). This proximity might explain why mutations at Asp^{31}/Gln^{62} in LptA have a strong influence upon thanatin binding (*vide supra*). In addition, the N-terminus of thanatin displays NOE contacts with residues from the loop of the opposite side of the ß-jellyroll (Gly^{78}-Gly^{82}). This loop is missing in the X-ray structure of free LptA (*9*) likely due to its flexibility. Finally, the side chains of thanatin Asn^{12} and Arg^{13} are likely involved in hydrogen bonding and formation of electrostatic interactions with LptA$_m$, respectively. The amide side chain protons of Asn^{12}, whose resonances are significantly downfield shifted in complex with LptA$_m$, are in a suitable geometry to form hydrogen bonds with the backbone carbonyl oxygen atoms of Ser^{40} and

Asp^{41}. The guanidinium groups of Arg^{13} and Arg^{14} in thanatin are within salt bridge distances to carboxylate groups in LptA$_m$ (Than.Arg^{13}-LptA$_m$.Glu^{39}, Than.Arg^{14}-LptA$_m$.Asp^{41}).

It has been shown that LptA can form head-to-tail homodimers *in vivo*, although it remains possible that a single LptA molecule can bridge the periplasm by contacting both LptC and N-LptD (Figure 1) (*7*). Furthermore, the known crystal structure of an LptA head-to-tail oligomer (PDB 2R1A) clearly reveals the N-terminal ß-strands of one subunit interacting with the C-terminal strands of the next LptA subunit (*9*). This interaction is likely important in assembling the LptA protein bridge across the periplasm in the macromolecular Lpt complex (Figure 1A). In addition, the N-terminal strands of LptA mediate binding of LptA to membrane anchored LptC (Figure 1) (*7, 9, 29, 30*). The NMR structure of LptA complexed with thanatin, reported here, superimposed upon the crystal structure of the LptA head-to-tail oligomer (PDB 2R1A), reveals that the thanatin binding site overlaps and would therefore block the interaction between LptA subunits (Figure 4D). It also seems likely that thanatin will inhibit the LptA/C protein-protein interaction. Finally, the C-terminal strands of LptA bind to the N-terminal ß-strands in the periplasmic ß-jellyroll domain of LptD. It is intriguing that the structure of the N-terminal ß-strands of the ß-jellyroll in LptD are highly similar to those in LptA (*14, 15*). Indeed, residues in LptA that contact thanatin in the complex are highly conserved in the same positions in LptD (see section-11, in SI). This strongly suggests that thanatin should interact with the N-terminal ß-strands in the ß-jellyroll of LptD/E. This implies that thanatin should also inhibit the interaction of LptA with LpD. Reported affinities of the LptA/LptA and LptA/LptC interactions have K_ds in the low micromolar range (*8, 31*). The nanomolar affinity of thanatin to both LptA and LptD reported here, therefore, appears strong enough to inhibit multiple protein-protein interactions required for assembly of the LPS trans-periplasmic protein complex.

These results highlight a new paradigm for an antibiotic action, targeting a dynamic network of protein-protein interactions required for assembly of the Lpt complex in *E. coli*. The results also identify one naturally occurring peptide as a starting point for the development of potential clinical candidates that target dangerous Gram-negative bacterial

pathogens. Finally, this work may also contribute to a better understanding of the biological function of thanatin in its natural context, in controlling titres of symbiotic or invading bacterial pathogens in the mid-gut of various insect species (*32*).

MATERIALS AND METHODS

Peptide synthesis

Methods of synthesis and analytical data for all peptides are included in the Supplementary Information (SI).

Methods for fluorescence and electron microscopy

Methods for fluorescence microscopy and transmission electron microscopy have been described in detail previously (*24*).

Photoaffinity labeling

E. coli ATCC25922 cells grown in MH-I broth (50 mL) to an OD_{600} of 1.0 were collected, washed once and taken up in PBS (50 mL) and incubated for 30 min at 37 °C with shaking at 200 rpm in the dark with 2-10 µg/ml thanatin-PAL5. Photoactivation was achieved by UV irradiation at 350 nm in a Rayonet Reactor (16 x 8W *Sylvania* blacklight lamps) for 30 min at 30 °C. Cells were then collected and washed two times with PBS. Cell pellets can be stored at -20 °C. The cell pellet was resuspended in 50 mM Tris-HCl, pH 7.3, with protease inhibitor cocktail (cOmplete™ *Roche*) and lysed by three cycles of sonication using a Branson digital sonifier equipped with a microtip (80 W, 30% intensity, 20 s on with 20 s off for 2 min) under cooling on ice. To remove unbroken cells and cell debris, the lysate was centrifuged (30 min at 4'000 rpm, 4 °C). The supernatant was subjected to ultracentrifugation (200'000 g, in a Sorvall T-875 rotor, 1 h, 4 °C). The pellet was washed with 50 mM Tris-HCl, pH 7.3 and collected again by ultracentrifugation (1 h, 4 °C).

Identification of photolabeled proteins by mass spectrometry

Photolabeled and PBS-washed *E. coli* were lysed in 50 mM ammonium bicarbonate (AmBic) containing protease inhibitor cocktail (*Roche*, cat: 11704900) and 0.1 % RapiGest (*Waters*, cat: 186002122) by six intervals of 30 s ultrasound sonication in a vial tweeter (*Hielscher Ultrasonics* GmbH) at a power of 170 W and 80% cycle time. Protein concentration was determined by Nanodrop 2000 Spectrophotometer (*Thermo Fisher Scientific* Inc.) and 10 mg protein was incubated with 200 µl streptavidin agarose resin (*Thermo*, cat: 53116) for 100 min at 4 °C to bind biotinylated proteins. Beads were settled by centrifugation at 2000 g for 5 min and transferred to Mobicol columns equipped with a 30 µm pore size filter (*MoBiTec* GmbH). Beads were extensively washed with 5 M NaCl, StimLys buffer (50 mM Tris pH 7.8, 137 mM NaCl, 150 mM Glycerol, 0.5 mM EDTA, 0,1 % Triton X-100, 100 mM $NaHCO_3$ and AmBic) to remove non-biotinylated proteins. Bead-bound proteins were reduced with 5 mM Tris(2-carboxyethyl)phosphine in AmBic for 40 min at 37 °C, alkylated with 10 mM iodoacetamide in AmBic for 30 min at 37 °C and proteolytically digested by sequencing grade modified trypsin (*Promega*, cat: V511A) at an enzyme to protein ratio of 1:100 for 20 h at 37 °C. Released peptides were acidified and subjected to C18 purification using UltraMicroSpin Columns (*The Nest Group*).

Peptide samples were separated by reversed-phase chromatography on a high-performance liquid chromatography (HPLC) column (75-µm inner diameter, *New Objective*) that was packed in-house with a 15 cm stationary phase (ReproSil-Pur C18-AQ, 1.9 micrometer) and connected to a nano-flow HPLC with an autosampler (EASY-nLC 1000, *Thermo Scientific*). The HPLC was coupled to a Q-Exactive plus mass spectrometer (*Thermo Scientific*) equipped with a nano electrospray ion source (*Thermo Scientific*). Peptides were loaded onto the column with 100% buffer A (99.9% H_2O, 0.1% FA) and eluted at a constant flow rate of 300 nl/min with a 30 min linear gradient from 6–20% buffer B (99.9% MeCN, 0.1% FA) followed by a 15 min transition from 20 to 32% buffer B. Electrospray voltage was set to 2 kV, sheath and auxiliary gas flow to zero and capillary

temperature to 250 °C. In data-dependent acquisition (DDA) mode the mass spectrometer automatically switched between precursor and fragment ion detection. Following a high-resolution survey mass spectrum (from 300 to 1,500 m/z) acquired in the Orbitrap with resolution R = 70,000 at m/z 200 (automatic gain control target value $3*10^6$), the 15 most abundant peptide ions with a minimum intensity of $2.5*10^4$ were selected for subsequent HCD fragmentation with an isolation window of 1.4 Da and fragments were detected by MS/MS acquisition in the Orbitrap at resolution R = 35,000 (automatic gain control target value $1*10^6$). Target ions already selected for fragmentation were dynamically excluded for 30 seconds.

Acquired raw files were subjected to protein identification using Comet (v.2015.01) and Trans Proteomic Pipeline v.4.7 (SPC/ISB Seattle) by matching ion spectra acquired in DDA mode against a SwissProt (UniProt consortium) reviewed *E. coli* protein database (downloaded Nov. 2016). Peptides were required to be fully tryptic with a maximum of 2 missed cleavage sites, carbamidomethylation as fixed modification and methionine oxidation as a dynamic modification. The precursor and fragment mass tolerance was set to 20 ppm and 0.02 Da, respectively. Identified proteins were quantified by integration of chromatographic traces of peptides using Progenesis QI v.2.0 (*Nonlinear Dynamics*, UK). Contaminant hits were removed and proteins filtered to obtain a false discovery rate of < 1%. Raw protein abundances based on non-conflicting peptides were exported and differential abundance testing was performed using R-package MSstats v3.5.3 (*33*). Significantly enriched *E. coli* proteins (abundance fold change ≥ 2 and adjusted p-value ≤ 0.05) were considered as bona fide Thanatin-PAL5 binding candidates. Mass spectrometric data were deposited to the ProteomeXchange Consortium (http://www.proteomexchange.org/) via the PRIDE partner repository (data set identifier: PXD-XXXX) (*to be deposited upon publication*).

Thanatin-resistant *E. coli* mutants

E. coli ATCC25922 was grown in MH-II broth (20 mL) to OD_{600nm}=1 at 37°C with 200 rpm shaking. This bacterial culture (100 µL, corresponding to ≈$5x10^7$ colony forming units) was

plated onto MH-II agar plates containing 10-50 µg/mL thanatin and incubated at 37 °C overnight. Growing colonies were then passaged at least four times over MH-II plates without selection on thanatin, and then MIC values against thanatin were determined. Two independent experiments were performed. Of the initial 10 isolates, the mutants Than^{R}-2, Than^{R}-4, Than^{R}-8, Than^{R}-9 and Than^{R}-10 exhibited stable resistance (MIC ≥64 µg/mL), and in each the *lptA* gene was sequenced, which revealed mutations Q62L or D31N in the primary sequence of the protein (Table S2). The antimicrobial activity of thanatin and seven standard antibiotics against the three selected mutants (Than^{R}-2, Than^{R}-4 and Than^{R}-8) are shown in Table S3.

The complete genomes of three selected mutants (Than^{R}-2, -4 and -8) as well as the wt (ATCC25922) strain used in these studies were sequenced using the Illumina MiSeq platform (MiSeq Reagent Kit v2, 500-cycles). Briefly, genomic DNA (gDNA) of the wt and the selected mutants was extracted using the *Sigma* NA2100 1Kit. One microgram of gDNA was sheared to 500 bp by sonication (*Covaris*). DNA fragments were further processed with the NEBNext Ultra II DNA Library Prep Kit for Illumina (NEB #E7645S/L). Genome mapping and identification of genetic variants was performed using CLC Genomics Workbench 10.1.1(CLC bio). The genes mutated in the resistant strains, compared to the wt, are shown in Table S4. In the Than^{R}-8 resistant strain, only a single bp change was found in the entire genome, in the *lptA* gene, corresponding to a Q62L change in the primary sequence of the protein.

Binding and NMR studies and structure determination of thanatin-LptA$_m$ complex

Production of LptA-His$_6$, LptA$_m$, LptD/E and thanatin in *E. coli* and details of binding assays with LptA by fluorescence polarization and thermophoresis are described in the SI (sections-8-10).

Production of [^{15}N]- and [^{15}N,^{13}C]-labelled LptA$_m$ was performed in BL21(DE3) *E. coli* cells grown in M9 minimal medium appropriately supplemented with $^{15}NH_4Cl$ and ^{13}C-glucose at 25 °C overnight. Purification is described in SI (section-8). The addition of 20 mM CHAPS to the sample buffer significantly improved the quality of the [^{15}N,^{1}H]-HSQC spectra by reducing line-broadening effects due to aggregation (see Figures S8 and S9). Final NMR samples contained 50 mM sodium phosphate, 150 mM NaCl, pH=7.5 and protein/peptide concentrations of 0.5-0.6 mM.

NMR spectra were acquired at 290 K (free ^{15}N-thanatin) and at 308 K (free ^{15}N,^{13}C LptA$_m$ and complex of LptA$_m$:thanatin) using 700- and 600-MHz Bruker Neo spectrometers. All spectra were processed using Topspin 4.0 and analyzed using Cara and CCPNmr. The ^{1}H, ^{15}N, and ^{13}C chemical shifts of backbone and side chain atoms were assigned using a standard set of triple resonance experiments on either uniformly ^{15}N,^{13}C-labeled LptA$_m$ with or without unlabeled thanatin, or with uniformly ^{15}N,^{13}C-labeled thanatin with or without unlabeled LptA$_m$ at protein concentrations of 0.5-0.6 mM. The LptA$_m$-thanatin complex was prepared at a ratio of 1:1.2.

Backbone assignment was initiated from manually picked [^{15}N,^{1}H]-HSQC spectra that served as anchoring points for HNCO, HN(CO)CACB and HNCACB experiments (*34*). Sequential resonance assignments used the standard strip matching procedure for Cα/Cβ chemical shifts. Backbone and side-chain chemical shift assignments were obtained for 89.7% and 85.7% of residues 28-143 of LptA$_m$ and 92.7% and 96.6% of residues 1-21 of thanatin, respectively. We noticed that resonances from the presumably unstructured C-terminal tail including the His-Tag (residues 144-170) as well as some residues in the longer loop regions (β6-β7) were often missing, likely due to accelerated amide proton exchange at pH 7.5. To this end, we adjusted the sample of the LptA:thanatin complex to pH 4.6, and re-measured the triple-resonance spectra. The overall signal dispersion in the [^{15}N,^{1}H]-HSQC spectra was not changed significantly, indicating a stable complex formation under those conditions. Additional amide cross peaks could be assigned to residues located in solvent-

exposed loops or strands, namely Gly^{30}, Gln^{43}, Met^{47}, Gly^{78}, Asp^{101} and Asp^{139}. Many more peaks became visible, that were often characterized by negative values of the $^{15}N\{^{1}H\}$-NOEs indicating that they belonged to flexible amide moieties, but that could not be assigned unambiguously.

Hβ and Hα chemical shifts obtained from the HBHA(CO)NH experiment were used in combination with Cα/Cβ chemical shifts from the backbone assignments to obtain sidechain assignments in HCCH experiments. The aromatic sidechains were linked to the backbone using the (HB)CB(CGCDCD)HD and (HB)CB(CGCDCDCE)HE experiments (*35*). The assignment of thanatin resonances in the complex was performed in a similar manner. Proton chemical shifts were referenced to the water line at 4.65 ppm at 308 K, from which the nitrogen and carbon scales were derived indirectly by using the conversion factors of 0.10132900 (^{15}N) and 0.25144954 (^{13}C). All chemical shifts were deposited in the BMRB database under ID 34261.

Upper-distance restraints used for the structure calculations of the $LptA_m$:thanatin complex were generated from 70 ms ^{15}N- and ^{13}C-NOESY (aliphatic and aromatic carbons) spectra. Intermolecular restraints were obtained from 70 ms $^{13}C,^{15}N$-filtered/^{13}C-edited (aliphatic & aromatic ^{13}C) and $^{13}C,^{15}N$-filtered/^{15}N-edited NOESY spectra, all experiments performed on two samples ($^{13}C,^{15}N$-labled $LptA_m$/unlabelled thanatin and unlabelled $LptA_m$/ $^{13}C,^{15}N$-labelled thanatin. Additional torsion angle restraints were derived from backbone chemical shifts using the program TALOS+ (*36*). The solution structure of the $LptA_m$:thanatin complex was determined using distance restraints derived from a set of NOESY spectra and torsion angle restraints derived from TALOS+. A full description of the structure calculations and statistical analysis of results are given in the SI.

References and Notes

1. A. Konovalova, D. E. Kahne, T. J. Silhavy, Outer Membrane Biogenesis. *Annu. Rev. Microbiol.* **71**, 539-556 (2017).
2. S. Okuda, E. Freinkman, D. Kahne, Cytoplasmic ATP Hydrolysis Powers Transport of Lipopolysaccharide Across the Periplasm in E-coli. *Science* **338**, 1214-1217 (2012).

3. S. Okuda, D. J. Sherman, T. J. Silhavy, N. Ruiz, D. Kahne, Lipopolysaccharide transport and assembly at the outer membrane: the PEZ model. *Nat. Rev. Microbiol.* **14**, 337-345 (2016).
4. D. J. Sherman *et al.*, Lipopolysaccharide is transported to the cell surface by a membrane-to-membrane protein bridge. *Science* **359**, 798-801 (2018).
5. P. Sperandeo *et al.*, Functional analysis of the protein machinery required for transport of lipopolysaccharide to the outer membrane of Escherichia coli. *J. Bacteriol.* **190**, 4460-4469 (2008).
6. A. X. Tran, M. S. Trent, C. Whitfield, The LptA protein of Escherichia coli is a periplasmic lipid-A-binding protein involved in the lipopolysaccharide export pathway. *J. Biol. Chem.* **283**, 20342-20349 (2008).
7. E. Freinkman, S. Okuda, N. Ruiz, D. Kahne, Regulated assembly of the transenvelope protein complex required for lipopolysaccharide export. *Biochemistry* **51**, 4800-4806 (2012).
8. J. A. Merten, K. M. Schultz, C. S. Klug, Conentration-dependent oligomerization and oligomeric arrangement of LptA. *Protein Sci.* **21**, 211-218 (2012).
9. M. D. L. Suits, P. Sperandeo, G. Deho, A. Polissi, Z. Jia, Novel structure of the conserved Gram-negative lipopolysaccharide transport protein A and mutagenesis analysis. *J. Mol. Biol.* **380**, 476-488 (2008).
10. C. Laguri *et al.*, Interaction of lipopolysaccharides at intermolecular sites of the periplasmic Lpt transport assembly. *Sci. Reps.* **7**, 13 (2017).
11. H. H. Dong, Z. Y. Zhang, X. D. Tang, N. G. Paterson, C. J. Dong, Structural and functional insights into the lipopolysaccharide ABC transporter LptB(2)FG. *Nat. Comm.* **8**, (2017).
12. Q. S. Luo *et al.*, Structural basis for lipopolysaccharide extraction by ABC transporter LptB(2)FG. *Nat. Struct. Mol. Biol.* **24**, 469-474 (2017).
13. I. Botos *et al.*, Structural and Functional Characterization of the LPS Transporter LptDE from Gram-Negative Pathogens. *Structure* **24**, 965-976 (2016).
14. H. H. Dong *et al.*, Structural basis for outer membrane lipopolysaccharide insertion. *Nature* **511**, 52-56 (2014).
15. S. Qiao, Q. S. Luo, Y. Zhao, X. J. C. Zhang, Y. H. Huang, Structural basis for lipopolysaccharide insertion in the bacterial outer membrane. *Nature* **511**, 108-111 (2014).
16. T. Wu *et al.*, Identification of a protein complex that assembles lipopolysaccharide in the outer membrane of Escherichia coli. *Proc. Natl. Acad. Sci. USA* **103**, 11754-11759 (2006).
17. P. Fehlbaum *et al.*, Structure-activity analysis of thanatin, a 21-residue inducible insect defense peptide with sequence homology to frog skin antimicrobial peptides. *Proc. Natl. Acad. Sci. USA* **93**, 1221-1225 (1996).
18. I. A. Edwards *et al.*, Contribution of Amphipathicity and Hydrophobicity to the Antimicrobial Activity and Cytotoxicity of beta-Hairpin Peptides. *ACS Infect. Dis.* **2**, 442-450 (2016).
19. Z. Hou *et al.*, Underlying Mechanism of In vivo and In vitro Activity of C-terminal-amidated Thanatin Against Clinical Isolates of Extended-Spectrum beta-lactamase-Producing Escherichia coli. *J. Infect. Dis.* **203**, 273-282 (2011).

20. B. Ma *et al.*, The Disulfide Bond of the Peptide Thanatin Is Dispensible for Its Antimicrobial Activity In Vivo and In Vitro. *Antimicrob. Agents Chemother.* **60**, 4283-4289 (2016).
21. Y. Shai, Mode of action of membrane active antimicrobial peptides. *Pept. Sci.* **66**, 236-248 (2002).
22. C. F. Le, C. M. Fang, S. D. Sekaran, Intracellular Targeting Mechanisms by Antimicrobial Peptides. *Antimicrob. Agents Chemother.* **61**, 16 (2017).
23. P. Rassam *et al.*, Supramolecular assemblies underpin turnover of outer membrane proteins in bacteria. *Nature* **523**, 333-340 (2015).
24. M. Urfer *et al.*, A Peptidomimetic Antibiotic Targets Outer Membrane Proteins and Disrupts Selectively the Outer Membrane in Escherichia coli. *J. Biol. Chem.* **291**, 1921-1932 (2016).
25. N. Srinivas *et al.*, Peptidomimetic Antibiotics Target Outer-Membrane Biogenesis in *Pseudomonas aeruginosa*. *Science* **327**, 1010-1013 (2010).
26. B. Van der Meijden, J. A. Robinson, Synthesis and application of photoproline - a photoactivatable derivative of proline. *ARKIVOC*, 130-136 (2011).
27. S. Chng *et al.*, Disulfide rearrangement triggered by translocon assembly controls lipopolysaccharide export. *Science* **337**, 1665-1668 (2012).
28. N. Ruiz, S. Chng, A. Hiniker, D. Kahne, T. Silhavy, Nonconsecutive disulfide bond formation in an essential integral outer membrane protein. *Proc. Natl. Acad. Sci. USA* **107**, 12245-12250 (2010).
29. A. X. Tran, C. Dong, C. Whitfield, Structure and Functional Analysis of LptC, a Conserved Membrane Protein Involved in the Lipopolysaccharide Export Pathway in Escherichia coli. *J. Biol. Chem.* **285**, 33529-33539 (2010).
30. K. M. Schultz, T. J. Lundquist, C. S. Klug, Lipopolysaccharide binding to the periplasmic protein LptA. *Prot. Sci.* **26**, 1517-1523 (2017).
31. K. M. Schultz, J. B. Feix, C. S. Klug, Disruption of LptA oligomerization and affinity of the LptA-LptC interaction. *Prot. Sci.* **22**, 1639-1645 (2013).
32. K. E. Park *et al.*, The roles of antimicrobial peptide, rip-thanatin, in the midgut of Riptortus pedestris. *Dev. Comp. Immunol.* **78**, 83-90 (2018).
33. M. Choi *et al.*, MSstats: an R package for statistical analysis of quantitative mass spectrometry-based proteomic experiments. *Bioinformatics* **30**, 2524-2526 (2014).
34. M. Sattler, J. Schleucher, C. Griesinger, Heteronuclear multidimensional NMR experiments for the structure determination of proteins in solution employing pulsed field gradients. *Prog. Nucl. Magn. Reson. Spectrosc.* **34**, 93-158 (1999).
35. T. Yamazaki, J. D. Kay, L. E. Kay, Two-Dimensional NMR Experiments for Correlating 13Cb and 1Hd/e Chemical Shifts of Aromatic Residues in 13C Labeled Proteins via Scalar Couplings. *J. Am. Chem. Soc.* **115**, 11054-11055 (1993).
36. Y. Shen, F. Delaglio, G. Cornilescu, A. Bax, TALOS+: a hybrid method for predicting protein backbone torsion angles from NMR chemical shifts. *J. Biomol. NMR* **44**, 213-223 (2009).
37. E. Michel, A. Plückthun, O. Zerbe, Peptide-Guided Assembly of Repeat Protein Fragments. *Angew. Chem. Int. Ed.* **57**, 4576-4579 (2018).
38. C. Massif *et al.*, New insights into water solubilization of fluorophores by post-synthetic "click" and Sonogashira reactions. *Organ. Biomol. Chem.* **10**, 4330-4336 (2012).

39. M. L. Cunningham, B. P. Kwan, K. J. Nelson, D. C. Bensen, K. J. Shaw, Distinguishing On-Target versus Off-Target Activity in Early Antibacterial Drug Discovery Using a Macromolecular Synthesis Assay. *J. Biomol. Screen.* **18**, 1018-1026 (2013).
40. S. Chng, N. Ruiz, G. Chimalakonda, T. Silhavy, D. Kahne, Characterization of the two-protein complex in Escherichia coli responsible for lipopolysaccharide assembly at the outer membrane. *Proc. Natl. Acad. Sci. USA* **107**, 5363-5368 (2010).
41. Z.-X. Wang, An exact mathematical expression for describing competitive binding of two different ligands to a protein molecule. *FEBS Lett.* **360**, 111-114 (1995).
42. B. J. Stockman, C. Dalvit, NMR screening techniques in drug discovery and drug design. *Prog. Nucl. Magn. Reson. Spectrosc.* **41**, 187-231 (2002).
43. P. Güntert, Automated NMR structure calculation with CYANA. *Methods Mol. Biol.* **278**, 353-378 (2004).
44. P. Güntert, L. Buchner, Combined automated NOE assignment and structure calculation with CYANA. *J. Biomol. NMR* **62**, 453-471 (2015).
45. N. Mandard *et al.*, Solution structure of thanatin, a potent bactericidal and fungicidal insect peptide, determined from proton two-dimensional nuclear magnetic resonance data. *Eur. J. Biochem.* **256**, 404-410 (1998).
46. C. D. Schwieters, J. Kuszewski, G. M. Clore, Using Xplor–NIH for NMR molecular structure determination. *Progr. NMR Spectrosc.* **48**, 47-62 (2006).

Acknowledgements

The authors thank Myriam Gwerder, the Center for Microscopy and Image Analysis at UZH, and the Functional Genomics Center Zurich for technical support. **Funding**: The following agencies are thanked for funding: M.M. and B.W. for ETH grant ETH-30 17-1 and Swiss National Science Foundation grant 31003A_160259; JAR was supported by the University of Zurich and the Swiss National Science Foundation grant 205320_146381. **Author Contributions**: S.V., K.Z., M.U., M.Mo., S.W., performed chemical and biochemical experiments, K.M and O.Z. conceived and performed NMR studies, K.Z, A.V., G.P. and L.E. conceived and performed genetic analyses, and M.Mu. and B.W. conceived and performed MS-based proteomic studies. All authors contributed to the analysis and interpretation of results, and J.A.R. wrote the paper, which was seen and agreed by all authors. **Competing interests**: Authors declare no competing interests. **Data and materials availability**: The PDB coordinates of the thanatin-LptA_m structure will be available in the PDB database after publication under accession number 6GD5. Mass spectrometric data will be available at the ProteomeXchange Consortium (http://www.proteomexchange.org/) via the PRIDE partner

repository (data set identifier: PXD-XXXX) (to be deposited after publication). All NMR chemical shifts will be deposited in the BMRB database under ID 34261.

Supplementary Materials.

Supplementary Information is available and describes: Strains and plasmids used; Synthesis and characterization of peptides; Methods and results of cell envelope permeabilization assays; Results of macromolecular synthesis assays; Methods of fluorescence microscopy and electron microscopy; Photoaffinity labeling methods including identification of photolabeled proteins by mass spectrometry; Methods and results obtained with thanatin-resistant mutants; Production and purification of recombinant proteins (LptA-His_6, $LptA_m$, LptD/E-His_6, thanatin); Binding assays by fluorescence polarization and thermophoresis; NMR structure determination.

Figures

Figure 1. **LPS Transport pathway and thanatin-based probes**. **A**, The LPS transport apparatus in Gram-negative bacteria comprises the seven proteins LptA-G, which form a macromolecular complex spanning the IM and OM. LPS transport across the periplasm occurs over a bridge formed by one or more copies of LptA. **B**, structures of thanatin and the photoprobe thanatin-PAL5 and fluorescence probe thanatin-BDP-FL.

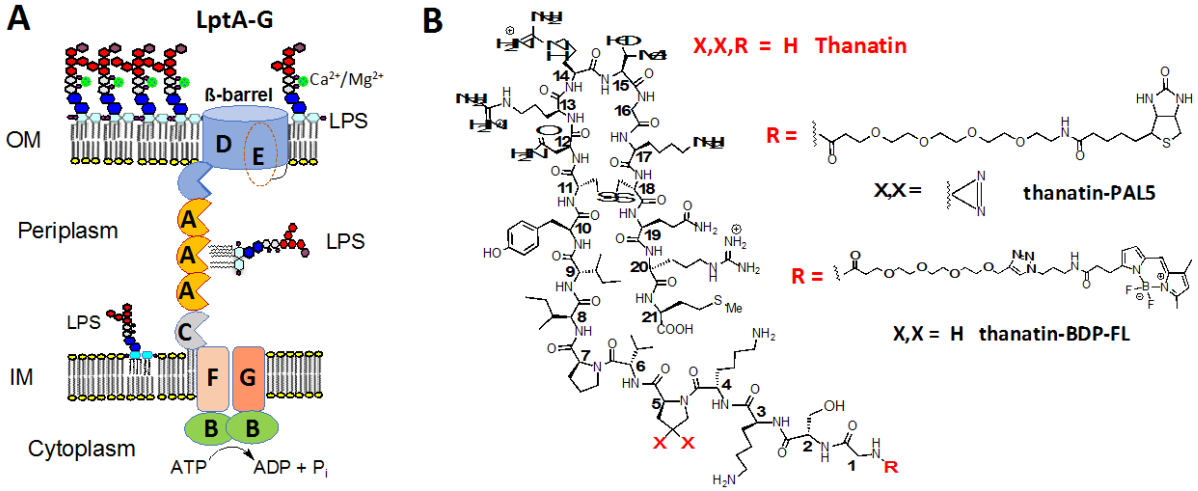

Figure 2.

Electron and fluorescence microscopy studies. A, B, TEM studies of *E. coli* ATCC25922, before (**A**) and after (**B**) thanatin treatment (1.5 µg/mL), showing internal accumulations of membrane-like material. Scale bar 500 nm. **C-D**, Super-resolution fluorescence microscopy of *E. coli* ATCC25922 without (**C**) or with thanatin (5 µg/mL, **D**) and stained with FM4-64, Sytox-Green, or DAPI. *Top* the FM4-64 channel (red staining); *bottom*, superimposition of all three channels (with DAPI (blue) and SYTOX-Green (non detected)). **E** (both pictures) *E. coli* staining with thanatin-BDP-FL (8 µg/mL) for 2 h at 30°C. Cells were analyzed using a Leica CLSM SP8 gSTED microscope. *Scale bars,* 4 µm; or bottom right 10 µm. For experimental details see Section-4, SI.

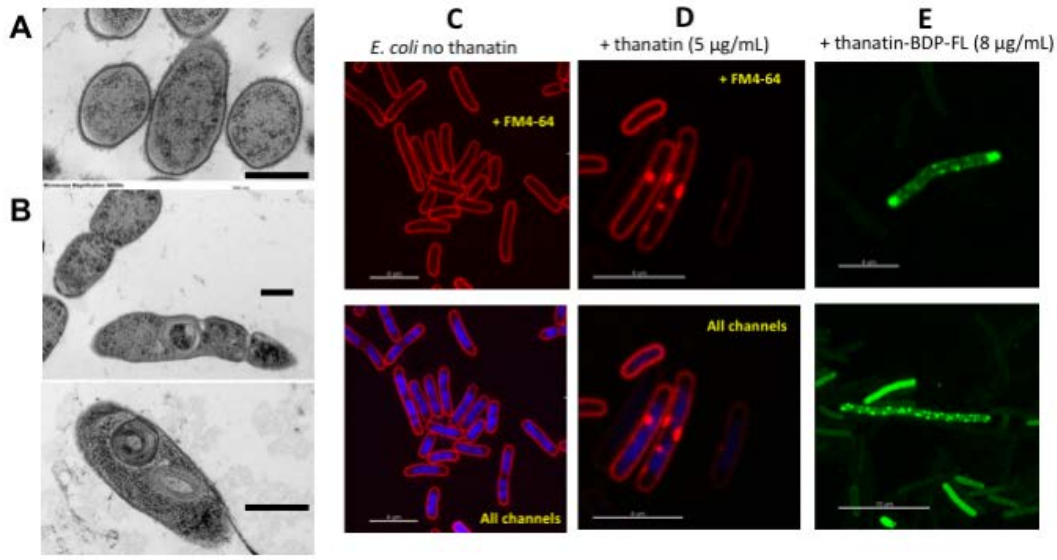

Figure 3.

Photolabeling *E. coli* ATCC25922 with thanatin-PAL5. A, Western blot (biotin detection) and corresponding SDS-PAGE (Coomassie blue staining) of membrane protein fraction from: *Lane-1*, control unlabeled cells; *Lane-2 and -3*, cells photolabeled with thanatin-PAL5 (10 µg/mL and 2 µg/mL); *Lane-4*, cells photolabeled with thanatin-PAL5 (10 µg/mL) + competitor thanatin (200 µg/mL). **B**, Western blot and SDS-PAGE after photolabeling with thanatin-PAL5 (2 µg/mL) with (+) or without (-) reduction of extracted membrane proteins with DTT. **C**, Volcano Plot showing relative abundance of *E. coli* proteins in thanatin-PAL5 labeled versus unlabeled control sample after streptavidin pulldown detected by MS-based proteomic analysis. Significantly enriched proteins (right/above dotted lines) are highlighted in green and represent PAL5-labeled proteins.

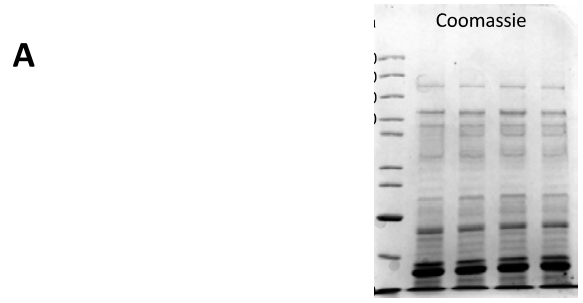

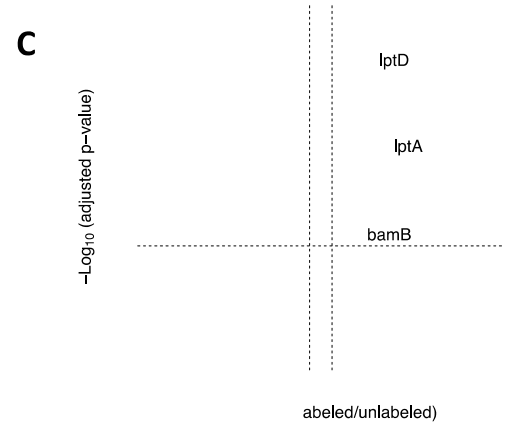

Figure 4.

The solution structure of the LptA$_m$-thanatin complex. (A) Ribbon representation of a single NMR LptA$_m$-thanatin complex in two different orientations. LptA$_m$ and thanatin are in green and red, respectively. The flexible C-terminus of LptA$_m$ encompassing residues 144-159 and the His-tag are not shown. (B) Structurally relevant intermolecular NOEs between backbone atoms of the first β-strands of LptA and thanatin are indicated with dotted arrows, and H^N-H^N and H^N-Hα NOEs are colored in blue and green, respectively. (C) Ribbon model of the LptA$_m$-thanatin complex. Residues involved in the protein-peptide hydrophobic interface (left panel) as well as in hydrogen bonding and electrostatic interactions (right panel) are indicated by ball-and-stick representation. (D) Superposition of the LptA dimer (PDB 2R1A, chains B (light blue) and C (violet) with the LptA$_m$-thanatin complex (green/red). Thanatin occupies a binding site on LptA$_m$ which is used to mediate LptA-LptA interactions needed to form the periplasmic bridge connecting inner and outer membranes for LPS transport.

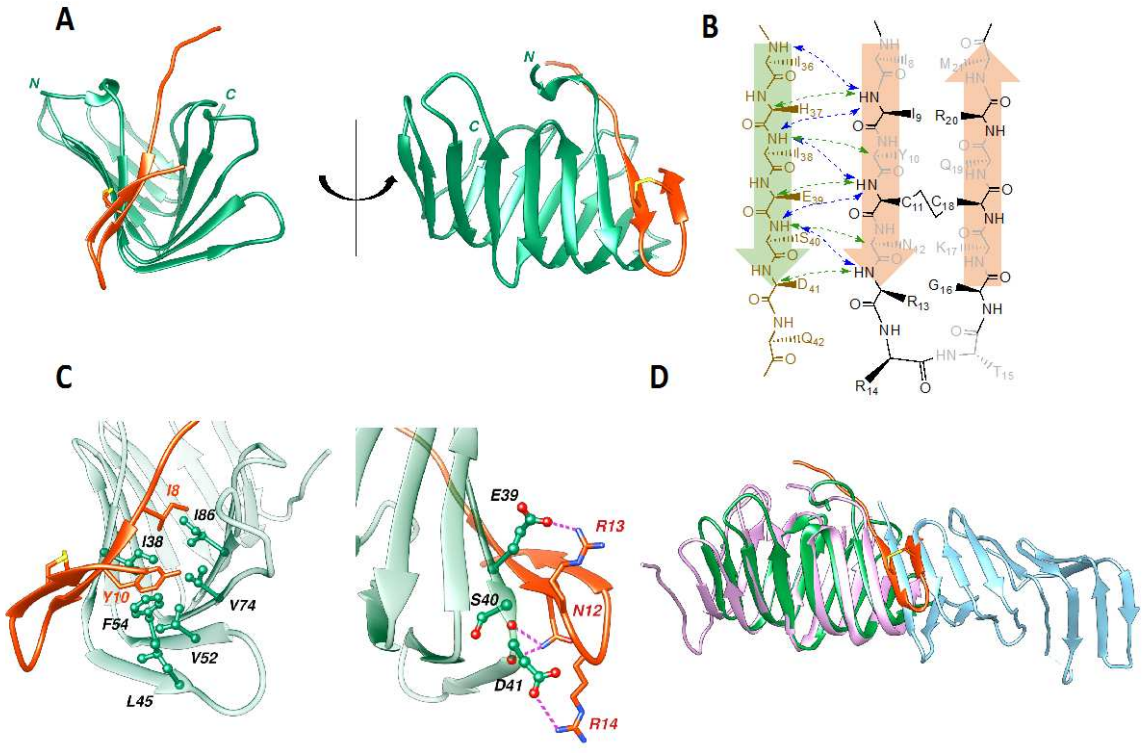

Supplementary Information for the article:

Thanatin Targets the Inter-Membrane Protein Complex Required for Lipopolysaccharide Transport in *Escherichia coli*

Stefan U. Vetterli[1], Katja Zerbe[1], Maik Mueller[3], Matthias Urfer[1], Milon Mondal[1], Shuang-Yan Wang[1], Kerstin Moehle[1], Oliver Zerbe[1], Alessandra Vitale[2], Gabriella Pessi[2], Leo Eberl[2], Bernd Wollscheid[3] & John A. Robinson[1]

[1] Chemistry Department, University of Zurich, Winterthurerstrasse 190, 8057 Zurich, Switzerland.

[2] Department of Plant and Microbial Biology, University of Zurich, Zollikerstrasse 107, 8008 Zurich, Switzerland.

[3] Institute of Molecular Systems Biology & Department of Health Sciences and Technology, ETH Zürich, Auguste-Piccard-Hof 1, 8093 Zürich, Switzerland.

Table of Contents

1. Bacterial strains and plasmids used in this study

Table S1. Bacterial strains and plasmids used in this study.

Bacterial strains used in this study	
E. coli ATCC25922	ATCC strain collection
E. coli XLI blue	ATCC strain collection
E. coli ML35 (ATCC 43827)	ATCC strain collection
E. coli BL21 (*DE3*)	Novagen
E. coli K12 MG1655 (ATCC 47067)	ATCC strain collection

Plasmids used in this study	description	reference
pET3a	-	Novagen
pUC19	-	New England Biolabs
pET22b	-	Novagen
pOCI1548	*lpt*A (1-185) *Nde*I/X*ho*I in pET22b	this study
pOCI1551	*lpt*A (1-185, Q61L) *Nde*I/*Xho*I in pET22b	this study
pOCI1551	*lpt*A (1-185, D31N) *Nde*I/*Xho*I in pET22b	this study
pET3a::*lpt*Am	*lpt*A (1-159) with C-terminal hexahistidine tag NdeI/BamI in pET3a	this study
pEMBT2	-	(*37*)
pEMBT2_thanatin	gene coding for Thanatin *Sap*I/*Bam*HI in pEMBT2	this study
pET3a::*lpt*D	*lpt*D *Nde*I/*Bam*HI in pET3a	this study
pCDFduet-1	-	Novagen
pCDF::*lpt*E-His6	*lpt*E with C-terminal hexahistidine tag *Nco*I/*Xho*I in pCDFduet-1	this study

2. Peptide Synthesis

Thanatin was synthesized by solid-phase peptide synthesis using standard Fmoc-chemistry, using the method described by Fehlbaum et al. (*17*). The disulfide bond was introduced by air oxidation in 0.1 M ammonium acetate buffer at pH 8.5. Crude peptide was purified by reverse phase HPLC (*Agilent* C18 column, 21.2 x 250 mm, 7 µm) using a binary gradient from 10 to 50% MeCN/H_2O with additional 0.1% TFA on an ÄKTA purifier 100 system (*Amersham Biosciences*). UPLC analysis was performed on an ACQUITY UPLC® system (*Waters*) equipped with a BEH130 C18 column, 2.1 x 100 mm, and 1.7 µm particle size at a gradient of 5 to 95% MeCN/H_2O with additional 0.1% TFA at 40°C. Enantiomeric D-thanatin was synthesized in the same way with D-amino acids. High resolution ESI-MS: m/z

487.4620 $[M+5H]^{5+}$ (native thanatin), m/z 487.4635 $[M+5H]^{5+}$ (D-thanatin), calc. mass 487.4616 $[M+5H]^{5+}$.

Synthesis of the photoprobes thanatin-PAL5 and thanatin-PAL7

The route used for synthesis of thanatin-PAL5 and thanatin-PAL7 is illustrated in Scheme S1, with thanatin-PAL5 as an example.

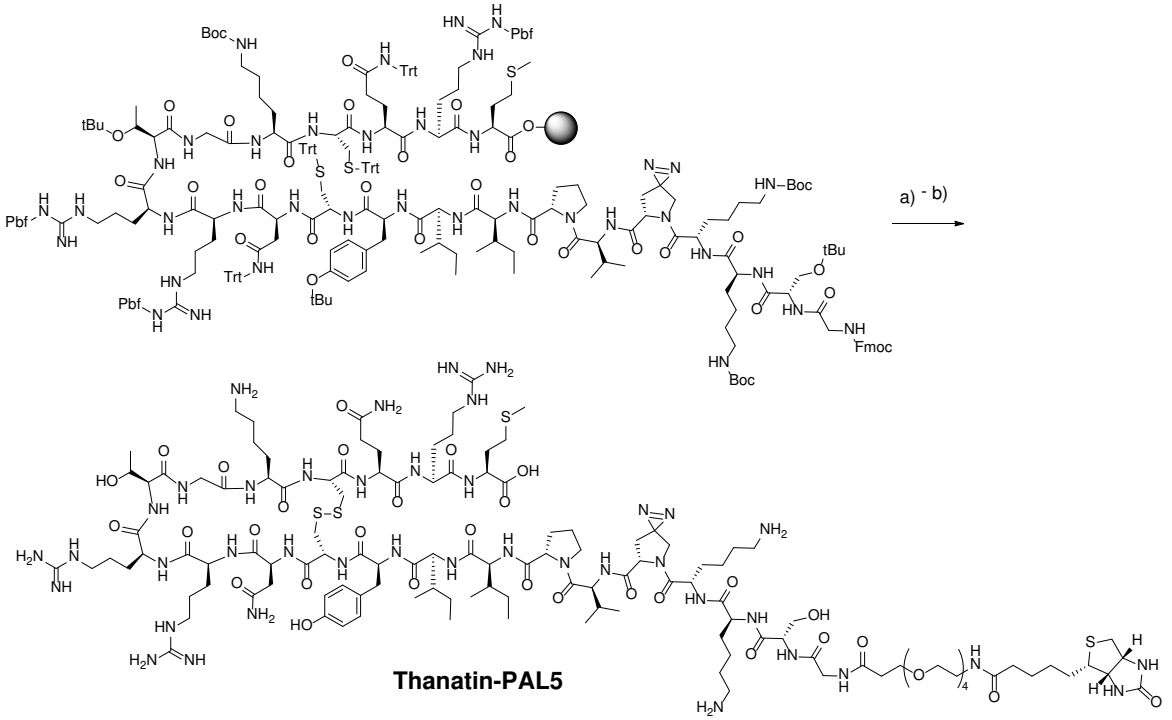

Scheme S1. **Synthesis of thanatin-PAL5**. The linear peptide was assembled by solid-phase peptide synthesis on chlorotrityl chloride resin using Fmoc chemistry. The synthesis of Fmoc-photoproline has been described elsewhere (*25, 26*). Resin-bound, side-chain protected linear peptide is shown, and was converted into thanatin-PAL5 in two steps: a) (*i*) Piperidine:DMF (1:3); then (*ii*) Biotin-PEG_4-COOH (*Broadpharm*), HATU, HOAt, DIPEA, DMF. b) (*i*) TFA:EDT:thioanisole:H_2O:TIS (75:10:10:4:1), then (*ii*) oxidation by air in 0.1 M ammonium acetate buffer, pH 8.5. Abbreviations: HATU, 2-(7-aza-1H-benzotriazole-1-yl)-1,1,3,3-tetramethyluronium hexafluoro-phosphate; DMF, dimethylformamide; HOAt, 1-Hydroxy-7-azabenzotriazole; DIPEA, diisopropylethylamine; TFA, trifluoroacetic acid; EDT. ethanedithiol; TIS, triisopropylsilane.

Incorporation of Fmoc-L-photoPro was performed according to published procedures (*26*). The linear thanatin sequence was synthesized as described above and then commercially available biotin-PEG_4-COOH (*Broadpharm*, Scheme S1) was coupled on-resin under standard conditions with HATU/HOAt. The peptide was then cleaved from the resin, deprotected, oxidized, and purified by preparative HPLC, as described above. After purification by HPLC, the purity of thanatin-PAL5 (>95%) was confirmed by UPLC and its identity by HR-ESI m/z (calc.) 587.3041 $[M+5H]^{5+}$, m/z (exp.) 587.3041 $[M+5H]^{5+}$. The sample showed antimicrobial activity against *E. coli* ATCC25922 (MIC of 2-4 µg/mL).

Synthesis of the fluorescent probe thanatin-BDP-FL

The fluorescent probe thanatin-BDP-FL was synthesized following Scheme S2. The linear thanatin sequence was synthesized on chlorotrityl chloride resin as described above. Commercially available propargyl-PEG_4-COOH (*Broadpharm*) was then coupled on-resin

under standard conditions with HATU/HOAt. After cleavage from the resin, deprotection, oxidation, and purification of the intermediate by preparative HPLC, BDP-FL-azide (*Lumiprobe*) was coupled by "click" chemistry (*38*). For this, the thanatin-PEG_4-alkyne intermediate (8.9 mg, 0.0033 mmol) was dissolved in H_2O (500 µl). Sodium ascorbate (35 µl, 0.1 M, 0.0035 mmol), BDP-FL-azide (0.0013 mmol, 0.25 mg) dissolved in DMSO (100 µl), and $CuSO_4$ (35 µl, 0.1 M, 0.0035 mmol) were sequentially added under stirring. After 30 min, the reaction mixture was injected directly on a preparative HPLC C18 column with a gradient of 10-50% MeCN/H_2O with additional 0.1% TFA. The isolated fraction was lyophilized yielding 4 mg (98%) of red lyophilisate. High resolution ESI-MS: m/z 763.1505 $[M+4H]^{4+}$ (Thanatin-BDP-FL) calc. mass 763.1500 $[M+4H]^{4+}$. The enantiomer D-thanatin-BDP-FL was made in exactly the same way using D-amino acids. HR-ESI-MS: m/z 763.1501 $[M+4H]^{4+}$.

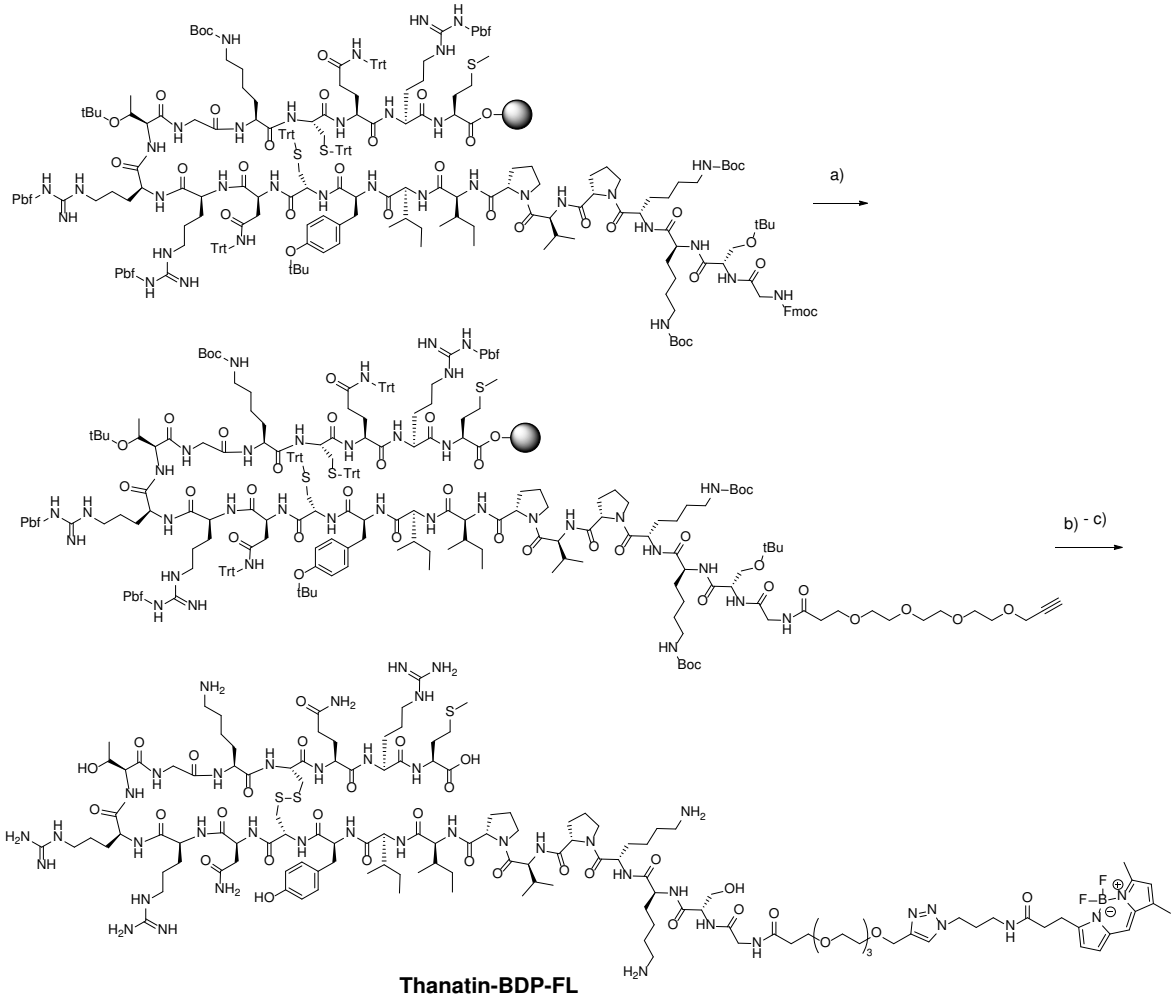

Thanatin-BDP-FL

Scheme S2. Synthesis of thanatin-BDP-FL. The linear peptide was assembled by solid-phase peptide synthesis on chlorotrityl chloride resin using Fmoc chemistry. a) (*i*) Piperidine:DMF (1:3), then (*ii*) propargyl-PEG_4-COOH (*Broadpharm*), HATU, HOAt, DIPEA, DMF. b) (*i*) TFA:EDT:thioanisole:H_2O:TIS (75:10:10:4:1), then (*ii*) oxidation by air in 0.1 M ammonium acetate pH 8.5. c) BDP-FL-azide (*Lumiprobe*), $CuSO_4$, sodium ascorbate, DMSO:H_2O (1:5).

L-Thanatin-BDP-FL showed good antimicrobial activity against *E. coli* ATCC25922 (MIC of 1- 2 µg/mL).

Synthesis of the fluorescent probe thanatin-Cy3

The intermediate thanatin-PEG_4-alkyne (9.3 mg, 0.0035 mmol) (Scheme S2, after step-b) was dissolved in H_2O (500 µl), and sodium ascorbate (0.1 M, 35 µl, 0.0035 mmol), Cy3 azide (*Lumiprobe*, 0.00174 mmol, 1 mg) dissolved in 100 µl DMSO and $CuSO_4$ (0.1 M, 35 µl, 0.0035 mmol) were added (Scheme S3). After 15 min the reaction mixture was injected directly on a preparative HPLC C18 column with a gradient of 20-60% MeCN/H_2O (0.1% TFA). The isolated fraction was lyophilized yielding 2.3 mg (41%) of purple lyophilisate. High resolution ESI-MS: m/z 643.5538 $[M+5H]^{5+}$ (Thanatin-Cy3), calc. mass 643.5531 $[M+5H]^{5+}$.

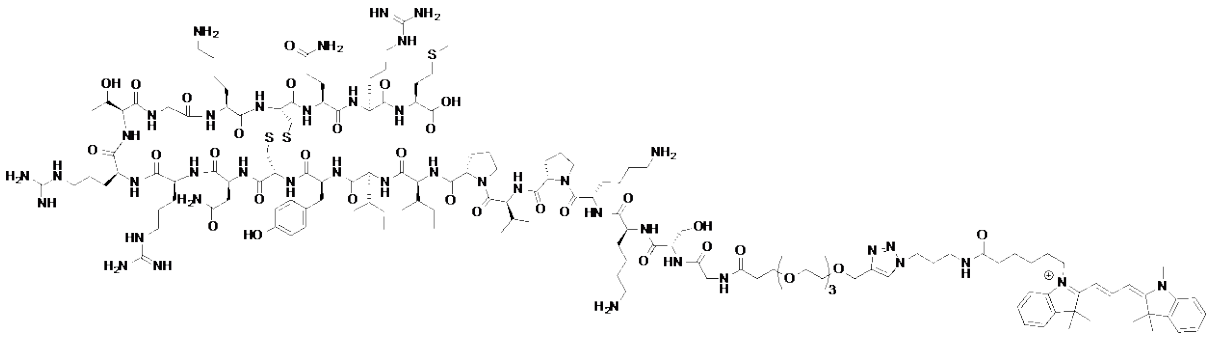

Scheme S3. **Structure of thanatin-Cy3.**

The enantiomer, D-thanatin-Cy3, was made in exactly the same way using D-amino acids. HR-ESI-MS m/z 643.5528 $[M+5H]^{5+}$.

3. Permeabilization of the *E. coli* cell envelope

E. coli with thanatin and Sytox-Green®

E. coli ATCC25922 was grown in Mueller-Hinton-I (MH-I) broth at 37 °C to an OD_{600} of 0.3-0.4. The cells were then centrifuged (5 min at 4000 rpm) and the pellet was resuspended in MH-I to an OD_{600} of 0.1. This culture was placed into a UV cuvette containing a magnetic stirring bar and 0.002% (w/v) of Polyoxethylene80 (Tween80). The fluorescence was recorded using an LS55 Fluorescence Spectrometer (*PerkinElmer*). Excitation and emission wavelength for Sytox-Green® dye are 488 nm and 525 nm respectively. After 100s, Sytox Green® dye (0.5 µM) was added from a stock solution (500 µM) in DMSO. After 400 s the antibiotic was added (arrow in Figure S1) and the fluorescence intensity was recorded. The effects of adding thanatin, polymyxin B and water (as control) are shown in Figure S1. At the same time the OD_{600} values were recorded at the start and end of the experiment. All measurements were performed in triplicate (error bars shown).

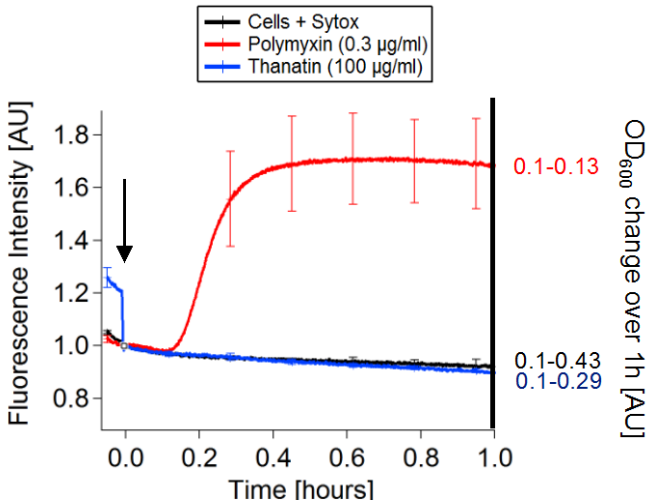

Figure S1. Membrane permeabilization monitored by uptake (or absence thereof) of SYTOX-Green®. No fluorescence increase is seen from cells in the presence of thanatin and SYTOX-Green®, or cells alone. The change in cell density (OD_{600}) in the cuvette over 1 h is shown on the right side. Note that substantial inhibition of growth is seen in the presence of thanatin at 100 µg/mL.

Release of ß-lactamase or ß-galactosidase from *E. coli* cells

A, Release of ß-lactamase from the periplasm was monitored using the substrate CENTA (*Merck-Millipore*, 180 µM) with *E. coli* ML35::pET3a grown in MH-II broth at 37 °C and resuspended in PBS with $CaCl_2$ (1 mM) and $MgCl_2$ (0.5 mM) and BSA (0.02% w/v). Hydrolysis of CENTA is monitored at 405 nm after addition of protegrin I, thanatin or ciprofloxacin at the concentrations shown (Figure S2, A). The green dashed lined is 100% lysis by sonication. **B**, Release of ß-galactosidase from the cytoplasm was monitored using the substrate *O*-nitrophenyl-ß-D-galactoside (250 µM) with *E. coli* ML53::pET3a grown in LB medium at 37 °C and resuspended in PBS with $CaCl_2$ (1 mM) and $MgCl_2$ (0.5 mM), and the antibiotics at the concentrations shown (Figure S2, B). All measurements were performed in triplicate (error bars shown).

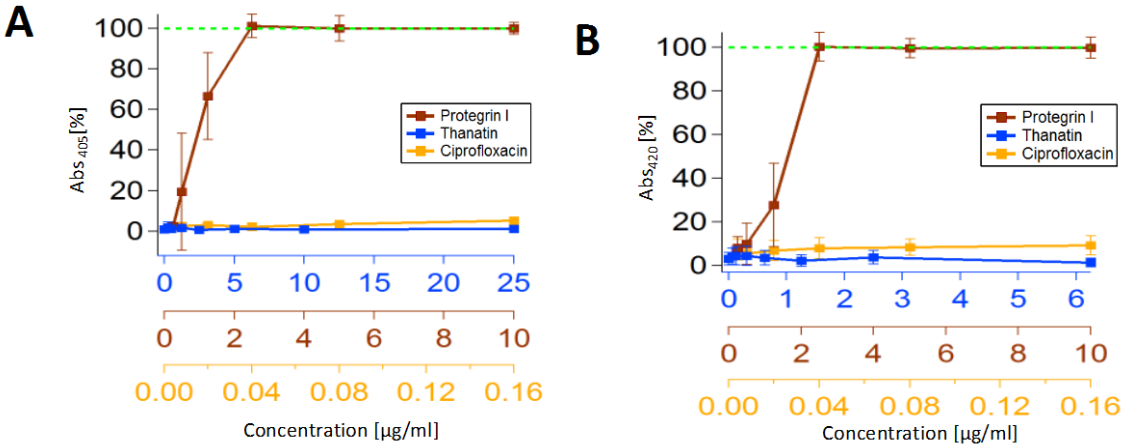

Figure S2. Release of ß-lactamase (**A**) and of ß-galactosidase (**B**) in the presence of antibiotic monitored by enzymic assays. Note that thanatin (and ciprofloxacin, as control) does not cause detectable release of either enzyme from cells, whereas protegrin I caused complete release of both enzymes (100% value corresponds to enzyme released by

sonication of cells).

4. Macromolecular synthesis assays

Macromolecular synthesis assays

The incorporation of radioactively labelled precursors ([^{3}H]-thymidine (80 Ci/mmol), L-[^{3}H]-leucine (108 Ci/mmol), [^{3}H]-uridine (30 Ci/mmol) or *N*-[^{3}H]-acetyl-glucosamine (30 Ci/mmol) into macromolecules (DNA, protein, RNA, or cell wall) in *E. coli* ATCC25922 was measured in chemically defined medium in a microplate format at various thanatin concentrations (*39*). Labelling was performed using exponentially growing cells at OD_{600} of 0.3 for 20 min. The incorporation of radioactivity relative to a control (no antibiotic) is shown in Figure S3. The experiment was performed in triplicate, and results from each experiment are shown.

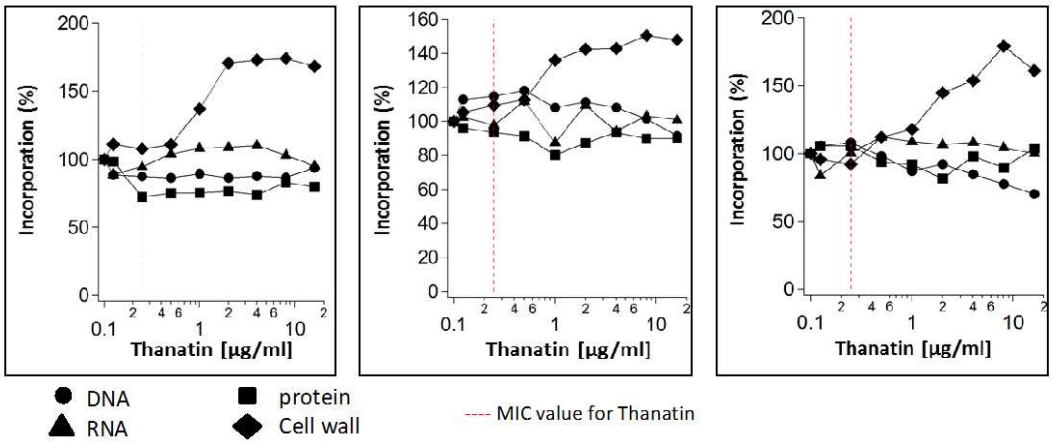

Figure S3. Relative incorporations of ^{3}H label from labelled precursor over 20 min, at 37 °C, performed in triplicate. The results show no inhibition of protein, RNA or DNA biosynthesis, but a slight stimulation of incorporation of N-[^{3}H]-acetylglucosamine, most likely into LPS, peptidoglycan or into polysaccharide capsule. In control experiments, the expected effects of known antibiotics inhibiting protein, DNA or RNA biosynthesis were observed (not shown).

5. Methods for fluorescence and electron microscopy

Methods for fluorescence microscopy and transmission electron microscopy have been described in detail previously (*24*).

6. Photoaffinity labeling

Detection of photolabeled proteins by Western blotting

Membrane protein fractions in SDS loading buffer containing DTT (100 mM) were boiled for 5 min at 100°C before SDS-PAGE under standard Laemmli conditions. Proteins were blotted to PVDF membrane (0.45 µm pore size, Immobilon®-P, *Merck*) using a 1:1 mixture of Tris-glycine-SDS (12 mM Tris, 96 mM glycine, 0.1% SDS) and phosphate-SDS-urea buffer (10 mM Na_2HPO_4, 1% SDS, 6 M urea). Blotting of proteins from gel onto the membrane was

achieved using a *Pierce* G2 Fast Blotter (*Thermo Fisher*) for 2 h at 0.5 A and 10 V. For chemiluminescence detection, the blocked membrane was incubated with Streptavidin-HRP or NeutrAvidin-HRP conjugate (*Pierce*, diluted 1:30'000 in PBS, 1% BSA, 0.2% Tween20) for 1 h. The membrane was washed 4 x 5 min with PBS and developed with WesternBright™ Sirius™ (*Advansta*) HRP substrate. Chemiluminescence was detected on a ChemiDoc™ MP Imaging System (*Bio-Rad*) over the course of 1-20 min.

7. Thanatin-resistant *E. coli* mutants

Of the initial 10 isolates (see text), the mutants Than^R-2, Than^R-4, Than^R-8, Than^R-9 and Than^R-10 exhibited stable resistance (MIC ≥64 µg/mL), and in each the *lptA* gene was sequenced, which revealed mutations Q62L or D31N in the primary sequence of the protein (Table S2). The antimicrobial activity of thanatin and seven standard antibiotics against the three selected mutants (Than^R-2, Than^R-4 and Than^R-8) are shown in Table S3.

Analysis of thanatin-resistant *E.coli* ATCC25922

	thanatin conc (µg/ml) on plate used for selection	MIC against thanatin (µg/ml)	MIC against thanatin (µg/ml) 4 generations later	Mutations found in LptA sequence	
WT		1-2	1-2		
Than^R-1	10	2-4	2	-	1st experiment
Than^R-2	50	>64	>64	Q62L	
Than^R-3	50	>64	1	-	
Than^R-4	50	32	64	D31N	
Than^R-5	20	16	4	-	
Than^R-6	20	16	4	-	
Than^R-7	20	16-32	1	n.d.	
Than^R-8	50	>64	>64	Q62L	2nd experiment
Than^R-9	50	>64	>64	Q62L	
Than^R-10	50	>64	>64	Q62L	

Table S2. Than^R isolates from two independent passaging experiments, with MICs against thanatin after 4 generations without selection pressure, together with point mutations detected by *lptA* sequencing.

MIC (µg/ml) in MH-II broth	E.coli ATCC 25922	ThanRes2 (LptA-Q62L)	ThanRes4 (LptA-D31N)	ThanRes8 (LptA-Q62L)
Colistin	0.06	0.03	0.06	0.015
Erythromycin	>64	>64	64	64
Gentamycin	0.5	0.5	0.5	0.5
Vancomycin	>64	>64	>64	n.d.
Rifampicin	8	8	8	16-64
Ampicilin	16	8	16	16
Ciprofloxacin	0.002	0.002	0.002	0.015
Thanatin	1	>64	>64	>64

Table S3. MIC values (µg/mL) of three selected mutants (Than^R-2, Than^R-4 and Than^R-8) and wt, against thanatin and seven standard antibiotics (colistin, erythromycin, gentamycin, vancomycin, rifampicin, ampicillin and ciprofloxaxin).

The genomes of Than^R-2, Than^R-4 and Than^R-8 were determined by genome sequencing. Mutations detected in the resistant strains, compared to the wt, are shown in Table S4. In the Than^R-8 resistant strain, only a single bp change was found in the entire genome, in the *lptA* gene, corresponding to a Q62L change in the primary sequence of the protein.

gene	Protein/Function	Than^R-2	Than^R-4	Than^R-8
lptA	LPS transport	+	+	+
rpmB	50S ribosomal protein 28L	+	-	-
pckA	Phosphoenolpyruvate carboxykinase	+	-	-
rplE	50S ribosomal protein L5	+	-	-
thiK	Thiamine kinase	+	+	-
acnB	Aconitate hydratase B	-	+	-
DR76_2839	unknown	+	+	-
DR76_4251	unknown	+	+	-
DR76_2319	unknown	+	-	-
DR76_3425	unknown	-	+	-

Table S4. Genes mutated in the mutant strain compared to wt (+ indicates a mutation, - indicates no mutation in the selected gene). Gene identifier and description were extracted from the GenBankfile CP009072.

For complementation experiments, genes encoding LptA with the corresponding mutations (Q62L-LptA-His$_6$ and D31N-LptA-His$_6$) were cloned into pET22b to give pOCI1551 or pOCI1552, respectively, with the empty pET22b plasmid and the plasmid containing the wild-type LptA-His$_6$ (pOCI1548) as controls. The plasmids were introduced into *E. coli* ATCC25922 or K12 MG1655. MIC values against thanatin show that both LptA mutants confer protection in both strains (Table S5).

	MIC against thanatin (µg/ml)		MIC against thanatin (µg/ml)
ATCC25922	0.5-1	*E.coli* K12	0.5-2
ATCC25922 + pET22b	0.25-0.5	*E.coli* K12 + pET22b	0.5-2
ATCC25922 + pOCI1551	32	*E.coli* K12 + pOCI1548	1-4
ATCC25922 + pOCI1552	16-8	*E.coli* K12 + pOCI1551	32- >64
		E.coli K12 + pOCI1552	16-64

Table S5. Antimicrobial activities of thanatin (MIC, µg/mL) against *E. coli* wt strains, and strains containing plasmids shown.

8. Production of LptA-His$_6$, LptA$_m$, LptD/E and Thanatin in *E. coli*

8.1. Production of *E. coli* LptA-His$_6$ and LptA$_m$

The primary sequence of LptA in *E. coli* K12 MG1655 as well as ATCC25922 is:

```
  1 MKFKTNKLSL NLVLASSLLA ASIPAFAVTG DTDQPIHIES DQQSLDMQGN VVTFTGNVIV
 61 TQGTIKINAD KVVVTRPGGE QGKEVIDGYG KPATFYQMQD NGKPVEGHAS QMHYELAKDF
121 VVLTGNAYLQ QVDSNIKGDK ITYLVKEQKM QAFSDKGKRV TTVLVPSQLQ DKNNKGQTPA
181 QKKGN
```

green, signal peptide; *blue*, segment removed in $LptA_m$.

The *lptA* gene from *E. coli* ATCC25922 was amplified by PCR using primers Ndefor and Xhorev (Table S6) and cloned into NdeI/XhoI sites in the plasmid pET-22b to give pOCI1548 encoding LptA-His_6.

primer name	5'-3' sequence
lptA_Ndefor	ATCTACATATGAAATTCAAAAACAAAC
lptA_Xhorev	TACGTCTCGAGATTACCCTTCTTCTGTGC
lptA159_SGRVEHis6rev	ACAATGGATCCTCAATGGTGGTGGTGGTGGTGCTCGACGCGGCCGCTGCGCTTGCC TTTGTCGCTGAAAGCC

primer name	5'-3' sequence
lptD_Ndefor	ATCTACATATGAAAAAACGTATCCCC
lptD_Bamrev	ACAATGGATCCTCACAAAGTGTTTTGATACG
lptE_Ncofor	TTACACCATGGGGCGATATCTGGCAACATTG
lptE_His6_Xhorev	TACGTCTCGAGTCAATGGTGATGATGGTGATGGTTACCCAGCGTGGTGGAGACGCG

primer name	5'-3' sequence
Thanatin_SapIfor	ATCTAGCTCTTCACAGGGTAGCAAAAAACCGGTGCCGATTATTTATTGCAACCGC
Thanatin_BamHIrev	ACAATGGATCCTTACATGCGCTGGCATTTGCCGGTGCGGCGGTTGCAATAAATAATCG

Table S6. Sequences of primers used for cloning experiments.

The primary sequence of expressed LpA-His_6 (linker in red followed by His_6-tag) is shown below:

```
28  VTGDTDQPIH IESDQQSLDM QGNVVTFTGN VIVTQGTIKI NADKVVVTRP GGEQGKEVID
88  GYGKPATFYQ MQDNGKPVEG HASQMHYELA KDFVVLTGNA YLQQVDSNIK GDKITYLVKE
148 QKMQAFSDKG KRVTTVLVPS QLQDKNNKGQ TPAQKKGNLE HHHHHH
```

LptA-His_6 was produced in *E. coli* BL21(DE3) grown in TB with 2% glycerol, induced at OD_{600} of 0.80 with IPTG (0.1 mM) and further growth at 16°C and 200 rpm overnight. LptA-His_6 was purified over a 5 mL Ni-NTA HiTrap column in 50 mM sodium phosphate, pH 8, 300 mM NaCl, 2% glycerol, 20 mM imidazole, and elution with the same buffer and 300 mM imidazole. Further purification using a 6 mL ResourceQ column (in 50 mM sodium phosphate, pH 8, 100 mM NaCl, 2% glycerol, 0 - 1 M NaCl) gave LptA-His_6 collected in the flow-through. Mass analysis of the purified protein by ESI-MS confirmed the expected molecular mass and showed that the signal sequence had been removed (*m/z* (obs.) =18360.55, *m/z* (calc. 18360.55).

A truncated form of *lptA* ($LptA_m$, Δ160-185) (*10*) was amplified using the primers Ndefor and lptA159SGRVEhis6rev and the product was cloned *Nde*I/*Bam*HI into pET3a to introduce a linker and a His_6 tag.

The primary sequence of $LptA_m$ (linker in red, followed by the His_6-tag) is shown below (native amino acid numbering)

```
 30          40          50          60          70
VTGDTDQPIH IESDQQSLDM QGNVVTFTGN VIVTQGTIKI NADKVVVTRP
 80          90         100         110         120
GGEQGKEVID GYGKPATFYQ MQDNGKPVEG HASQMHYELA KDFVVLTGNA
130         140         150       159
YLQQVDSNIK GDKITYLVKE QKMQAFSDKG KRSGRVEHHH HHH

Green, linker; Red, His6 tag
```

$LptA_m$ was produced in LB medium after induction with 0.1 mM IPTG at OD_{600} of 0.6, overnight at 20°C. The purification was performed over a 5 ml Ni-NTA HiTrap column in 50 mM sodium phosphate, pH 8, 300 mM NaCl, 10% glycerol, 5 mM imidazole and elution with 500 mM imidazole in the same buffer. Mass analysis of the purified protein by ESI-MS confirmed the expected molecular weight and showed that the signal sequence had been removed (*m/z* (obs.) =15870.5, *m/z* (calc.) =15870.70).

8.2. Production of the *E. coli* LptD/E_{His} complex

The LptD/E complex was produced by slight adaptation of published procedures (*14, 15, 40*). The *E. coli lptD* including its native signal sequence was amplified by PCR using lptD_Ndefor and lptD_Bamrev primers (Table S6) and cloned *Nde*I/*Bam*HI into pET3a (*Novagen*) to give pET3a::lptD. Upon expression in *E. coli* and cleavage of the signal peptide, LptD has the native N-terminus (res. 23–784). *E. coli lptE* was amplified using the primers lptE_Ncofor and lptE_His6_Xhorev (Table S6) and cloned into *Nco*I/*Xho*I sites in the pCDFduet-1 vector (*Novagen*) with its native signal sequence to give pCDF::lptE-His.

Both plasmids were introduced into *E. coli* BL21(DE3) and coexpression of LptD and $LptE_{His}$ was achieved by selection with carbenicillin and streptomycin. Briefly, a 500 mL culture was grown at 26 °C until OD_{600} 0.8, then 0.1 mM IPTG was added and the culture was grown at 26 °C for another 22 h. Cells were pelleted by centrifugation at 5000 rpm, 4 °C for 30 min and then resuspended in 30 mL TBS (20 mM Tris-HCl, 150 mM NaCl, pH 8.0) containing 1 mM EDTA, 2 mM PSMF, and 1 mM benzamidine. The resuspended cells were lysed by sonication. The cell lysate was centrifuged at 5'000 rpm, 4 °C for 1 h to remove unbroken cells, and the supernatant was centrifuged at 45'000 rpm, 4 °C for 1 h to collect the total cell membranes, which were washed with TBS containing 0.5% N-lauroylsarcosine (25 mL) at 4 °C for 1 h in order to remove inner membranes. Outer membranes were collected by ultracentrifugation at 45'000 rpm, 4 °C for 1 h, extracted with 15 mL TBS-B (20 mM Tris-HCl, 100 mM NaCl, 20 mM imidazole, pH 8.0) containing 1% anzergent 3–14 at 4 °C for 2 h, and re-centrifuged as above.

The resulting supernatant was loaded onto a 5 mL HisTrap HP column (*GE Healthcare*), which was pre-equilibrated with TBS buffer containing 1% anzergent 3–14 (TBS-A). The flow through was collected and reloaded onto the column. The column was washed with 25 mL TBS buffer containing 0.02% anzergent 3–14 followed by 25 mL TBS containing 1% n-octylglucoside (OG) (TBS-B) and then eluted with TBS-C (20 mM Tris-HCl, 100 mM NaCl, 200 mM imidazole, pH 8.0) containing 1% OG.

The eluate was loaded onto a 6 mL Resource Q column (*GE Healthcare*), which was pre-equilibrated with Tris buffer (TB) (20 mM Tris-HCl, pH 8.0) containing 1% OG. The flow

through was collected and re-loaded onto the column. The unbound proteins were washed out with 24 mL TB containing 1% OG and proteins were eluted by a 180-mL gradient, 0 – 1000 mM NaCl in TB containing 1% OG. The fractions containing LptD/E_{His} were pooled and concentrated in an ultrafiltration device (*Amicon* Ultra, 50 kDa cut-off) to about 300 µL, and further purified by gel filtration on a prepacked Superdex 200 Increase 10/300 GL column (*GE Healthcare*), using TBS containing 1% OG as the eluent.

The LptD/E_{His} complex was analyzed by SDS-PAGE, after boiling to dissociate and unfold the complex, either with reduction by DTT (lane-2) or without DTT treatment (Figure S4). The Coomassie-stained gel shows the characteristic shift in mobility of LptD with the change in redox status of the disulfide bonds in LptD (*27, 28*).

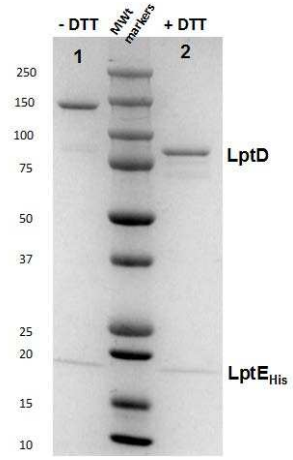

Figure S4. SDS-PAGE of purified LptD/E_{His} complex from *E. coli*. *Left*, without reduction of disulfide bonds with DTT; *right*, with reduction with DTT; *center*, molecular weight markers.

8.3. Production of labelled thanatin in *E. coli*

In order to produce [^{13}C,^{15}N]-labeled thanatin in *E. coli*, the gene coding for thanatin was synthesized from overlapping primers (Thanatin_SapIfor and Thanatin_BamHIrev, Table S6) and cloned into pEM3BT2 (kindly provided by E. Michel (*37*)). Production of uniformly labelled [^{13}C,^{15}N]-thanatin from *E. coli* BL21 (DE3):pEMBT2_thanatin in M9 minimal medium supplemented with 5 g/L $^{15}NH_4Cl$ and 5 g/L ^{13}C glucose was induced at OD_{600} 0.7 with 0.1 mM IPTG and the cells were grown overnight at 37°C.

After cell lysis the His_6-tagged fusion protein GB1-thanatin was purified by IMAC (1mL HisTrap cartridge, 50mM Na phosphate, 300mM NaCl, pH 7.5, 20-300mM imidazole). TEV cleavage was performed in dialysis using TEV cleavage buffer (50mM Tris pH 7.5, 0.5mM EDTA, 1mM DTT) and His-tagged TEV protease (ca. 12mM). Thanatin was collected by Ni-affinity purification in a washing step with 20mM imidazole. After dialysis in 0.1M ammonium acetate, pH 8.5, the oxidized thanatin was purified by C18 reversed phase HPLC (*Agilent Eclipse* XBD-C18) using a gradient of 10 to 50 % acetonitrile in H_2O in the presence of 0.1% TFA over 5 column volumes.

The composition of the NMR sample was the following:
380 µM [^{13}C,^{15}N]-thanatin and 1.2 eq $LptA_m$ (460 µM in 18 mM sodium phosphate buffer, pH 7.5, 54 mM NaCl, 20 mM CHAPS, 10% D_2O).

Sequence of the resulting GB1-thanatin fusion protein:

```
1  MSGSHHHHHH SSGIEGRGRQ YKLILNGKTL KGETTTEAVD AATAEKVFKQ YANDNGVDGE
61 WTYDDATKTF TVTESSGENL YFQGSKKPVP IIYCNRRTGK CQRM
```

(*Green*, His-tag; *blue*, GB1; *red*, thanatin; underlined, TEV cleavage site, between QG)

Cleavage of the fusion protein with tobacco etch virus (TEV) protease and air oxidation gives native thanatin.

9. Binding assays with LptA by fluorescence polarization and thermophoresis

9.1. Fluorescence polarization (FP)

FP measurements were recorded on a Safire^2 plate reader (*Tecan*) in black, flat-bottom, non-binding 96 well plates (*Greiner*). Instrument settings were optimized for Thanatin-BDP-FL (Excit. 470 nm, Emiss. 508 nm) with a bandwidth of 10 nm and a G-factor of 1.21, at room temperature. For the synthesis of the probe see Section-2.

Direct assay. In the direct assay a constant concentration of thanatin-BDP-FL (100 nM) was titrated with the analyte protein LptA-His$_6$. A 24-fold titration series of LptA-His$_6$ was prepared starting from 31 µM to 3.7 pM in buffer (sodium phosphate 50 mM, NaCl 150 mM, pH 8.0) and 0.05% Tween20. After incubation for 30 min, FP was recorded (Figure S5**A**). Data were averaged from triplicate experiments and normalized from the concentration point with the lowest anisotropy value. Data were fitted to a 1:1 binding model using GraphPad Prism by implementing equation E 1, where a = -1, b = K_d + x + A_{tot} and c = -x * A_{tot}. m is the amplitude of maximal anisotropy increase, K_d is the dissociation constant and A_{tot} is the total ligand concentration. The results (Figure S5**A**) gave a K_d 12 ± 3 nM for LptA-His$_6$ binding to thanatin.

$$y = m*((- b + sqrt(b^2 - 4*a*c)) / 2*a) / A_{tot} \qquad \text{E 1}$$

A

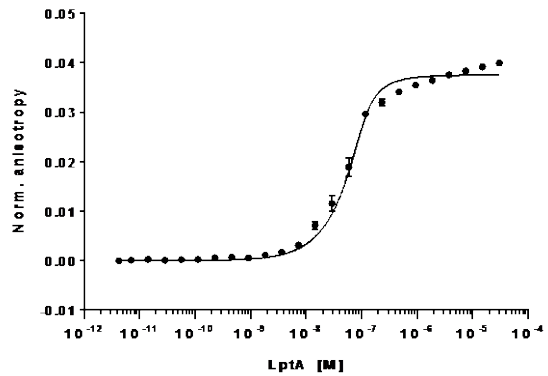

B

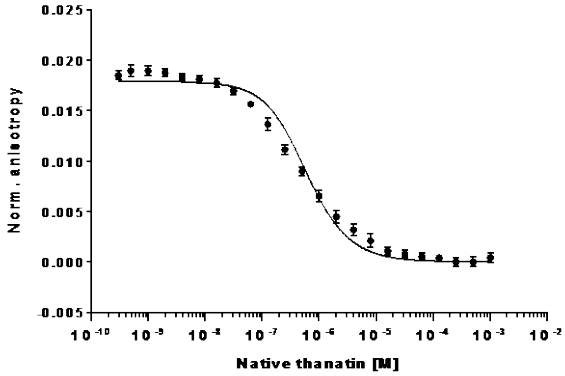

C

D

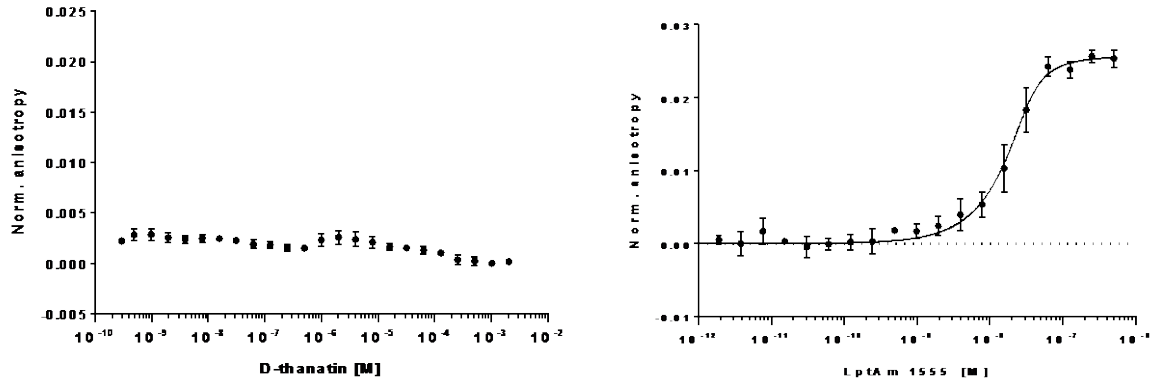

Figure S5. **A**, Direct FP binding assay of thanatin-BDP-FL (100 nM) titrated with the analyte protein LptA-His_6. Measurements were done in triplicate with standard deviation shown. **B,C**, Competition FP assay. The thanatin-BDP-FL (0.5 µM) and LptA-His_6 (0.5 µM) was titrated with free thanatin (**B**), or with enantiomeric D-thanatin (**C**) (no competition observed). Measurements were done in triplicate with standard deviation shown. **D**, FP assay reveals binding of thanatin-BDP-FL (30 nM) to $LptA_m$. Measurements were done in triplicate with standard deviation shown.

Competition assay. In the competition experiments, a constant concentration of thanatin-BDP-FL (0.5 µM) and LptA-His_6 (0.5 µM) was titrated with free thanatin, or with enantiomeric D-thanatin. After incubation for 30 min, FP was recorded (Figure S5**B,C**). Data were averaged from triplicate experiments and normalized from the concentration point with the lowest anisotropy value. Data were fitted to a competition binding model using GraphPad Prism by implementing methods described elsewhere (*41*), which gave a K_d for thanatin binding of 10 ± 2 nM.

Binding studies were also performed to show that thanatin binds to $LptA_m$. Using the same FP method (see above) and $LptA_m$, a K_d for binding to Thanatin-BDP-FL was determined (K_d ≈ 3.8 ± 1.0 nM) (Figure S5**D**).

9.2. Thermophoresis binding assays

The binding of thanatin to LptA-His_6 and to $LptA_m$ was quantified by Microscale Thermophoresis using a Monolith NT.115 instrument (*NanoTemper Technologies*) with hydrophobic capilliaries at room temperature in PBS (sodium phosphate (50 mM), NaCl (150 mM, pH 8.0), Tween-20 (0.05%). The protein was labeled with Dylight 650-N-hydroxysuccinimide ester labeling kit (*Thermofischer*). The results (Figure S6) gave a K_d 20 ± 1 nM for LptA-His_6 and 4.0 ± 0.24 nM for $LptA_m$.

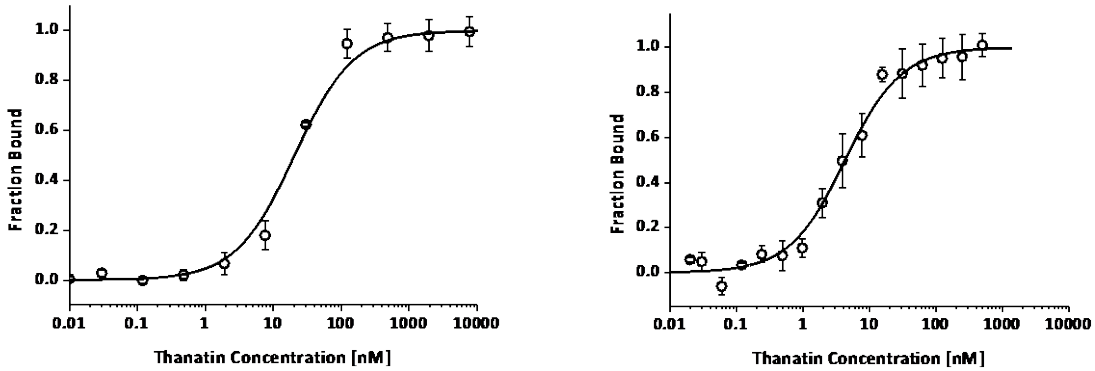

Figure S6. Binding of thanatin to LptA-Dylight650 (*left*) and $LptA_m$-Dylight650 (*right*) by Microscale Thermophoresis. Measurements were done in triplicate with standard deviation shown.

10. Binding assays with LptD/E by fluorescence polarization and thermophoresis

The binding of thanatin (and its enantiomer) to $LptD/E_{His}$ was studied by fluorescence polarization using thanatin-BDP-FL and by thermophoresis using thanatin-Cy3 (see Section 2).

Fluorescence polarization (FP)

FP measurements were performed on a plate reader (*Tecan* Safire Spectrometer) equipped with a FP module and a filter set for an excitation wavelength of 470 nm and emission of 508 nm with a band width of 10 nm. The fluorescently labelled thanatin-BDP-FL at 30 nM was titrated with $LptD/E_{His}$ from 1250 to about 0.0003 nM in TBS buffer (20 mM Tris-HCl, 100 mM NaCl, pH 8.0) with 1% w/v octylglucoside (OG) at 20 °C. The responses were analyzed using a standard Langmuir binding model, which gave a K_d of 34 ± 5 nM (Figure S7**A**). In addition, binding of the enantiomer D-thanatin-BDP-FL was also monitored to $LptD/E_{His}$. However, FP changes could only be detected with micromolar concentrations of $LptD/E_{His}$, and the upper plateau of the binding isotherm could not be reached. We conclude that the thanatin retains an ability to bind enantioselectively to the recombinant *E. coli* $LptD/E_{His}$ complex *in vitro*.

Thermophoresis

For thermophoresis studies, the fluorescently labeled thanatin-Cy3 (and its enantiomer) were used, with a Monolith NT.115 instrument (*NanoTemper Technologies*) with premium capillaries at RT. The thanatin-Cy3 concentration at 50 nM was titrated with $LptD/E_{His}$ in TBS buffer with 1% OG, pH 8, at RT, from 1000 to 0.06 nM, which gave a low but reproducible positive thermophoresis signal (Figure S7**B**). The responses were analyzed using a standard Langmuir binding model, from which an apparent $K_d \approx 44 \pm 27$ nM was determined. The enantiomeric form D-thanatin-Cy3 showed a *negative* thermophoresis signal, which increased into the micromolar range without reaching a stable plateau at the highest $LptD/E_{His}$ concentrations tested.

In addition, when thanatin-Cy3 was titrated with LptD/E_{His} an increase in fluorescence signal was observed (Cap scan) (Figure S7**C**). A K_d was also calculated from the normalized fluorescence and found to be 40 ± 8 nM. In contrast, D-thanatin-Cy3 showed an increase in fluorescence upon binding to the protein only at micromolar concentrations of LptD/E_{His}. Since an upper plateau could not be observed, a reliable K_d for this interaction could not be derived.

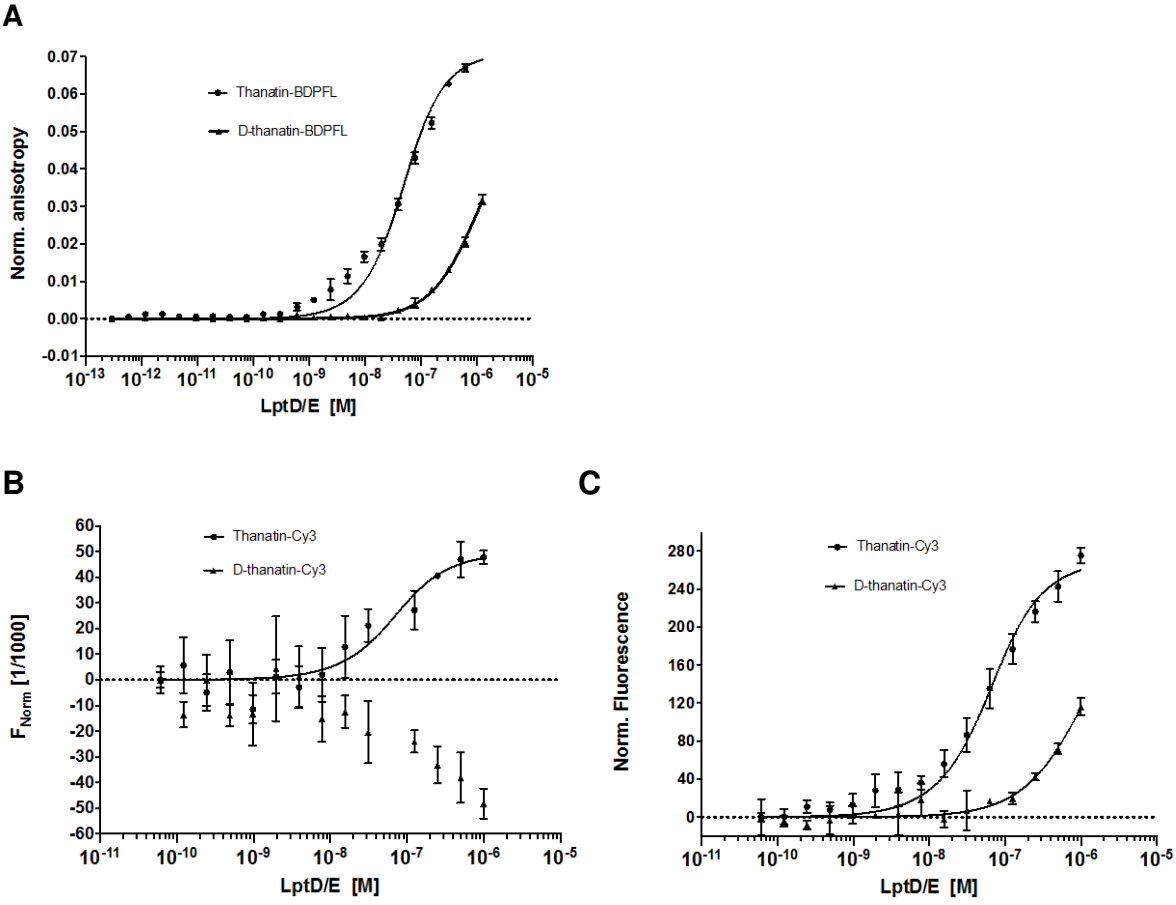

Figure S7. **A**, FP assay of thanatin-BDP-FL and D-thanatin-BDP-FL binding to LptD/E_{His} in TBS buffer with 1% OG. **B,C**, Binding assays to LptD/E_{His} using a Monolith NT.115 instrument (*NanoTemper Technologies*) recording both changes due to the thermophoresis effect (**B**), and total fluorescence changes (**C**), with both thanatin-Cy3 and D-thanatin-Cy3. Measurements were done in triplicate with standard deviation shown.

11. NMR studies and structure determination of thanatin-LptA_m complex

Annotated [^{15}N,^{1}H]-HSQC spectra are shown in Figures S8 and S9 for LptA_m or thanatin in free and complexed states. Note that numbering of LptA refers to the full-length sequence including the signalling sequence. Therefore, residue 28 in these annotations corresponds to the first residue of LptA_m after removal of the signal sequence.

Figure S8. Assigned [^{15}N,^{1}H]-HSQC spectra of ^{15}N-labeled LptA$_m$ in free form (*top*) and after addition of 1.2 equiv. of unlabeled thanatin (*center*). The *bottom* panel shows the overlay of both spectra. The complex is depicted with red contours.

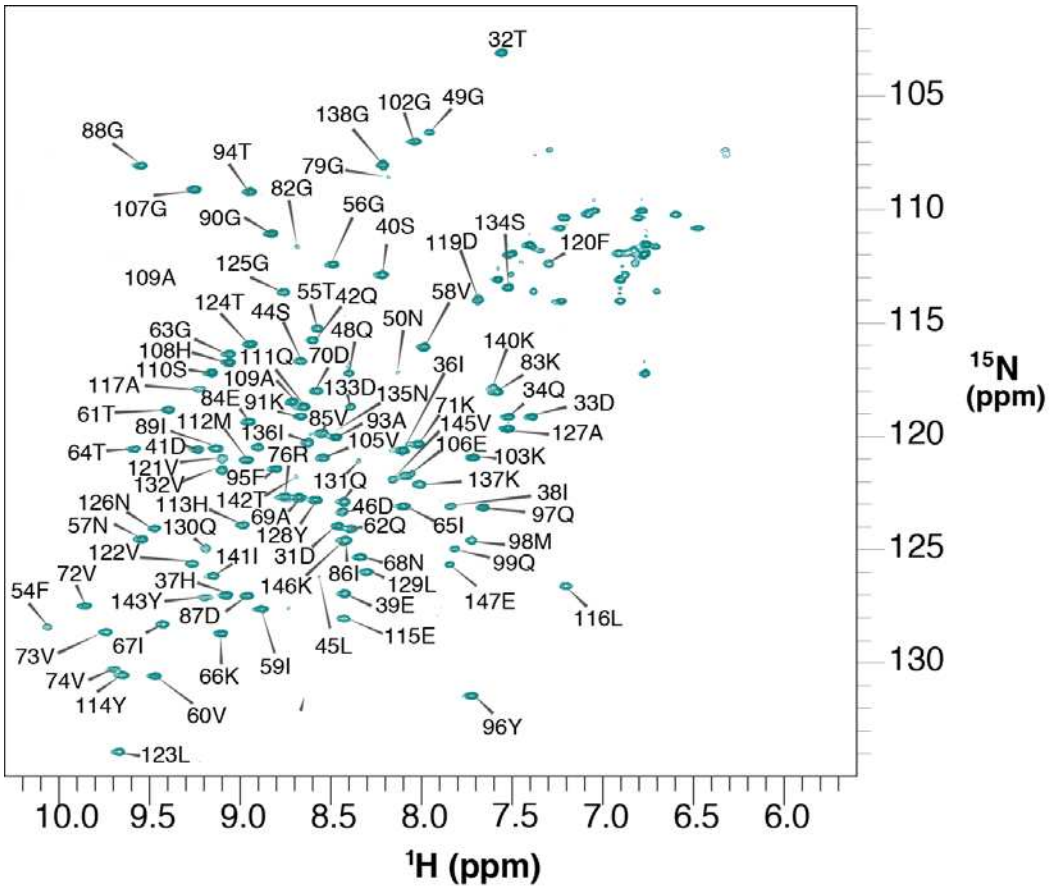

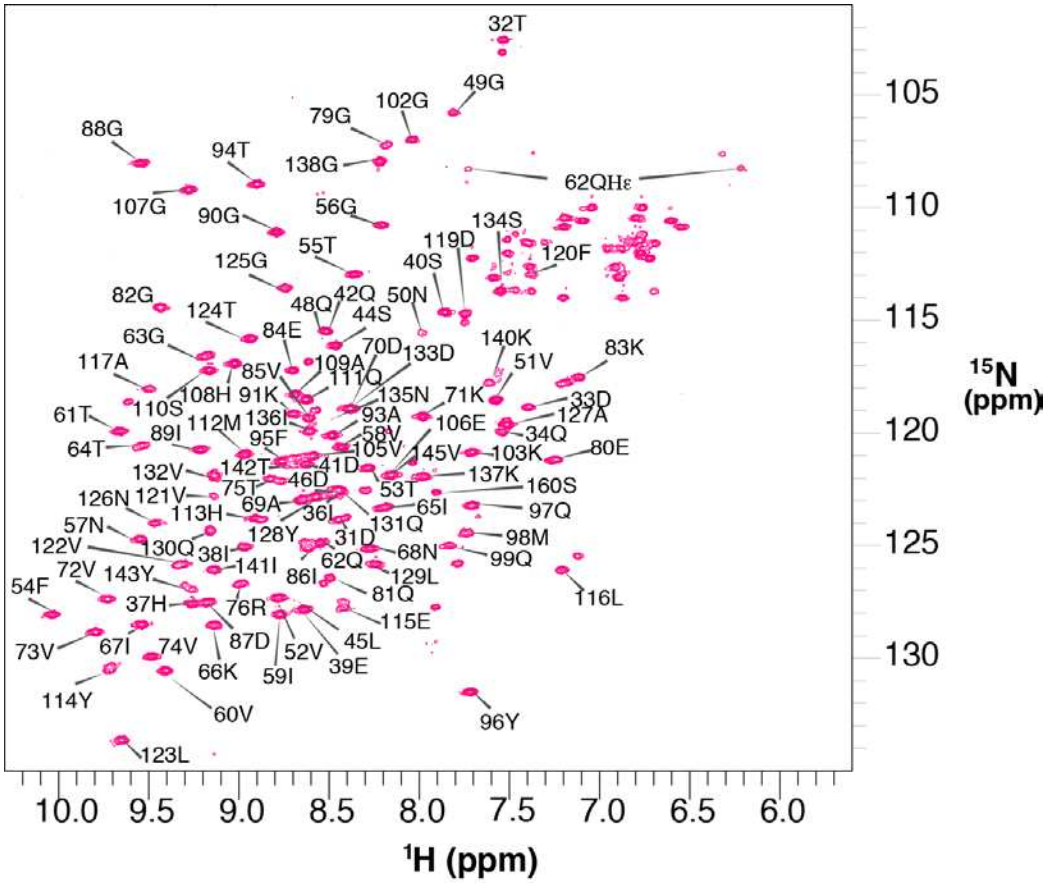
32T
49G
102G
79G
88G
94T
138G
62QHε
107G
90G
56G
134S
119D
55T
120F
125G
40S
82G
124T
48Q
42Q
50N
44S
84E
63G
70D
133D
140K
83K
117A
85V
109A
51V
111Q
108H
91K
135N
71K
33D
110S
61T
112M
136I
93A
106E
127A
89I
95F
58V
34Q
64T
105V
145V
103K
80E
132V
142T
41D
137K
46D
160S
75T
53T
126N
121V
69A
65I
97Q
113H
36I
131Q
57N
128Y
31D
98M
122V
130Q
38I
68N
99Q
72V
141I
62Q
129L
54F
143Y
86I
81Q
116L
37H
76R
115E
73V
67I
74V
87D
52V
45L
66K
59I
39E
114Y
60V
96Y
123L
105
110
115
120
125
130
15N
(ppm)
10.0
9.5
9.0
8.5
8.0
7.5
7.0
6.5
6.0
1H (ppm)

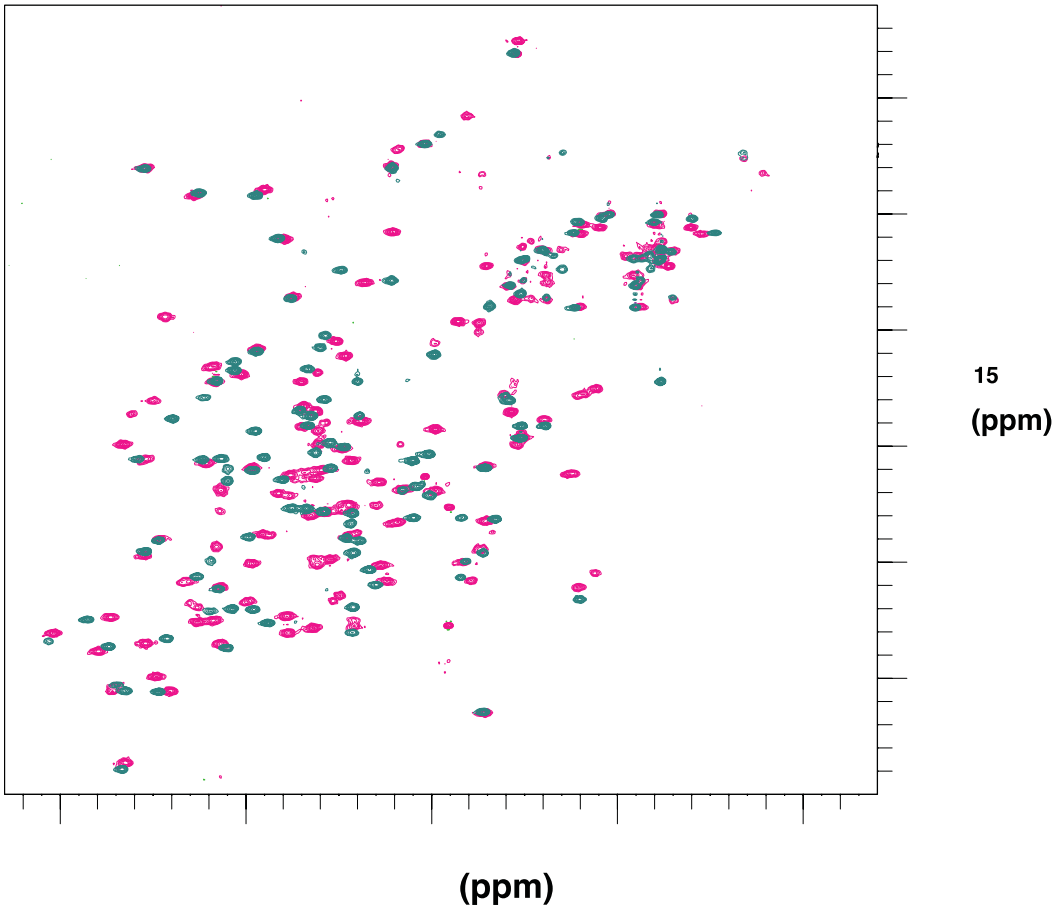
15
(ppm)
(ppm)

Figure S9. [^{15}N,^{1}H]-HSQC spectra of ^{15}N-labeled thanatin in free form (**A**) and after addition of 1.2 equiv. of unlabeled LptA$_m$ (**B**). The bottom panel shows the overlay of both spectra. The complex is depicted with red contours. In the PDB coordinates 6GD5 of the complex the first residue of thanatin has residue number 201

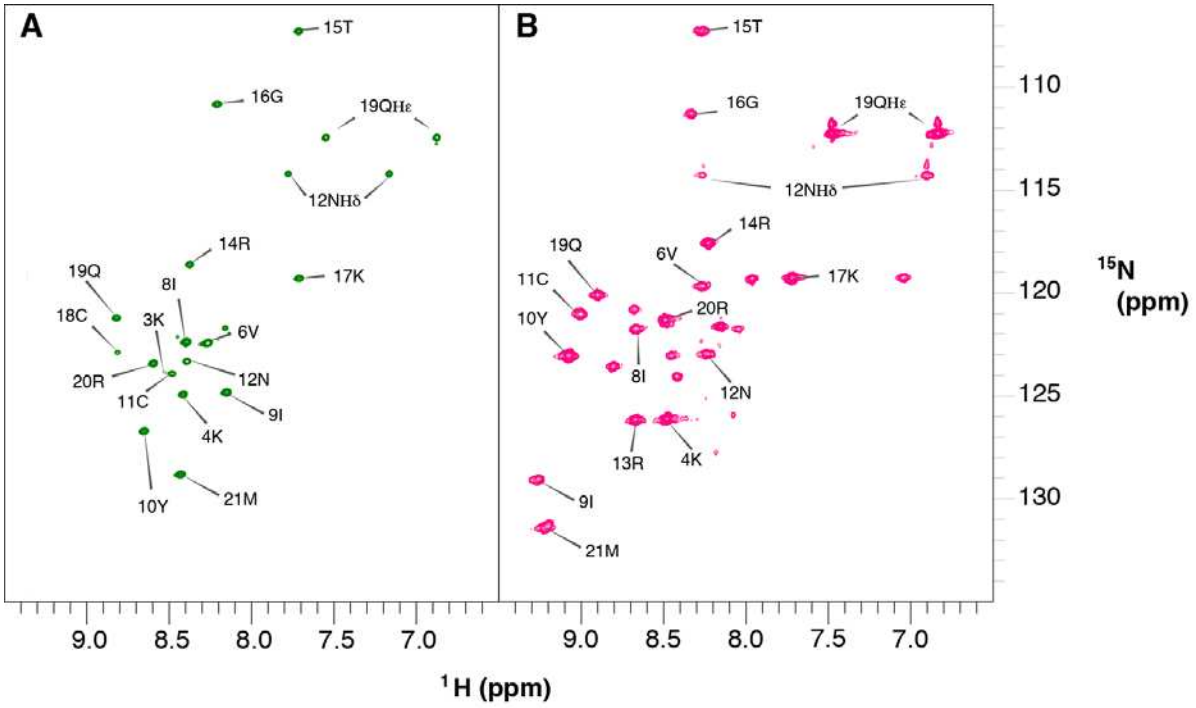

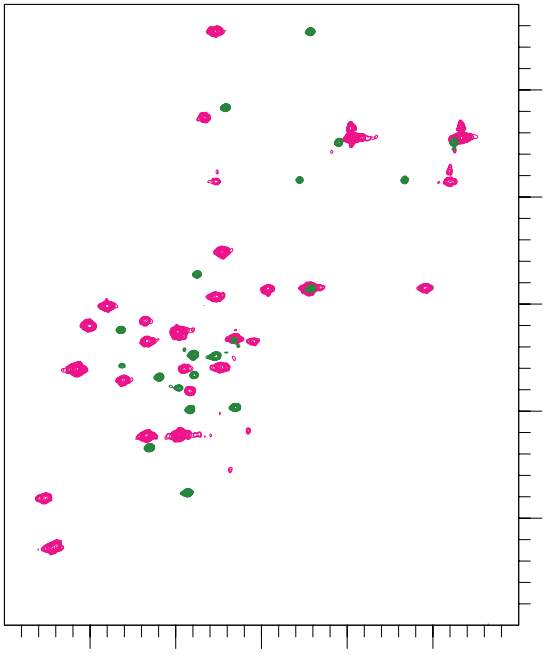

NMR Binding site studies

Chemical shift perturbations between the free and thanatin-bound $LptA_m$ were calculated according to

$$\Delta\delta = \sqrt{(^1H_f - ^1H_b)^2 + 0.2(^{15}N_f - ^{15}N_b)^2}$$

in which subscripts f and b denote free and complexed states (*42*) (Figure S10).

Figure S10. Weighted ^{15}N,^1H chemical shift changes ($\Delta\delta$) between the free and thanatin-bound $LptA_m$ as a function of residue number.

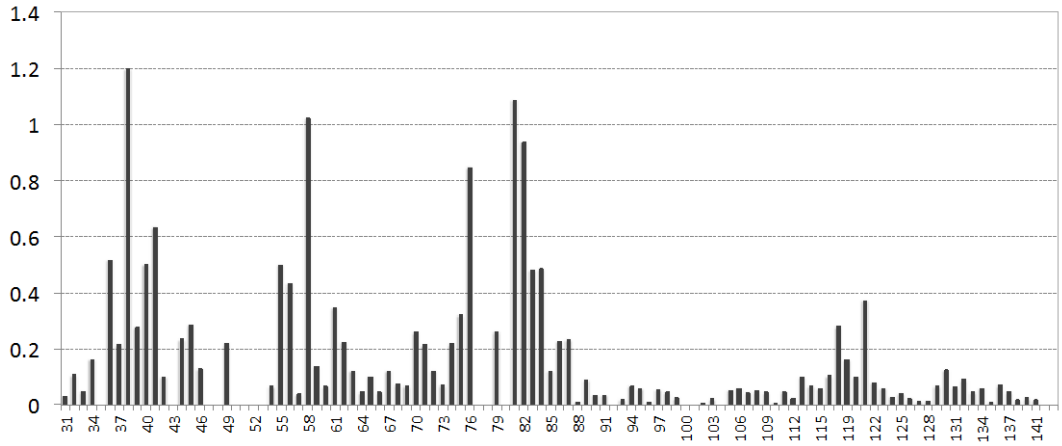

NOE analysis, structure calculations and refinement

The solution structure of the $LptA_m$:thanatin complex was determined using distance restraints derived from a set of NOESY spectra (*vide supra*) and torsion angle restraints derived from TALOS+. TALOS+ predicted 14 β-strands and a short N-terminal α-helix (Figure S11) but yielded no unambiguous predictions for the C-terminal segment (144-170) and the loop region connecting strands β6 and β7. Unassigned peak lists were annotated using the "noeassign" macro of CYANA 3.97 (*43, 44*), which in an iterative fashion matches peaks to known chemical shifts, and attempts to resolve ambiguous assignments based on preliminary structure calculations and network anchoring. To improve convergence of the calculations, the coordinates of the first noeassign cycle were initially replaced by a model complex based on the X-ray structure of *E. coli* LptA (pdb code 2R1A) (*9*) and the solution structure of thanatin (pdb code 8TFV) (*45*). Two different starting orientations (parallel and anti-parallel beta-sheet complementation) of thanatin were tested. When the model was not supplied after the first cycle the computed structure was similar, but the resolution was lower because some long-range NOEs were not correctly identified. Nevertheless, it was very clear that the beta strands of $LptA_m$ and thanatin complemented each other in a parallel fashion. Once the overall topology was clear, NOESY spectra were manually inspected and many more interfacial long-range NOEs identified.

In total, 1085 NOE upper distance restraints distributed through residues 29-139 of $LptA_m$ and residues 2-21 of thanatin were applied in the final structure calculations. During the simulated annealing procedure 202 dihedral angle restraints derived from TALOS were applied. The target-function of the 20-lowest energy conformers was about 1.7. Finally, the 20 lowest CYANA conformers were refined in explicit water using the CHARMM22

parallhdg5.3 force-field as implemented in XPLOR-NIH (*46*). The scripts from the xplor-nih-tutorial-2014/gb1_rdc distribution were utilized for refinement. Important parameters of the structure calculation, the refinement, and superposition RMSDs as well as figures for the quality of the obtained structures are presented in Table S7.

The final bundle of 20 low energy structures for $LptA_m$-thanatin complex reveals good definition of the structured parts of $LptA_m$ (residues 30-143) and thanatin (residues 4-20) (Figure S11), characterized by a backbone RMSD of 0.8 ± 0.2 Å. 99.7% of the ϕ/ψ dihedral combinations are located in the most favoured regions of the Ramachandran plot and only 0.4% in the disallowed regions. A summary of the structure calculation statistics is given in Table S8. The coordinates of the structured parts are deposited in the pdb database under accession code 6GD5.

Figure S11. Ribbon representation of the 20 lowest-energy NMR conformers in two different orientations. Backbone atoms of residues 30-143 were superimposed. The flexible C-terminus of LptA encompassing residues 144-170 is not shown. $LptA_m$ and thanatin are depicted in green and red, respectively.

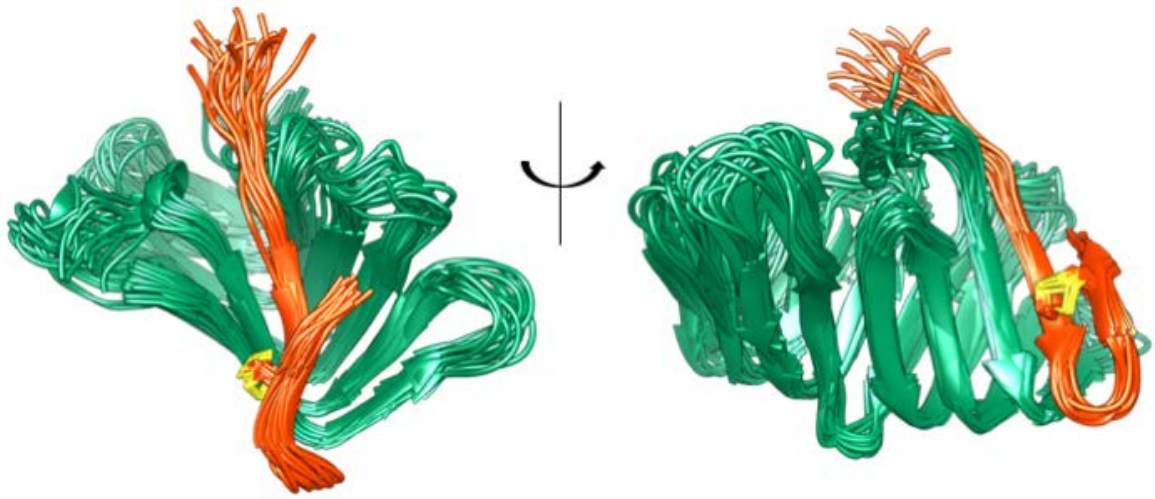

Comparison of the jellyroll domains in LptA and LptD

Based on a sequence and structure alignment of the N-terminal ß-strands in the β-jellyroll domain of LptD and the β-jellyroll of LptA it can be seen that residues of LptA involved in thanatin binding are identical or similar in LptD (Figure S12).

Figure S12. (*Top*) Sequence alignment of LptA (res. 28-76) and LptD (res. 43-91). Residues in LptA interacting with thanatin in the complex (Figure S11) are marked with stars. (*Bottom*) Superimposition of LptD N-terminal domain (from the crystal structure PDB 4Q35, res. 43-91, blue) with LptA (crystal structure PDB 2R1A, res. 28-76, chain C, violet) shown in the sequence alignment (*Top*). The side chains of residues which are situated in the thanatin binding site (Figure S11) are displayed in ball-and-stick representation.

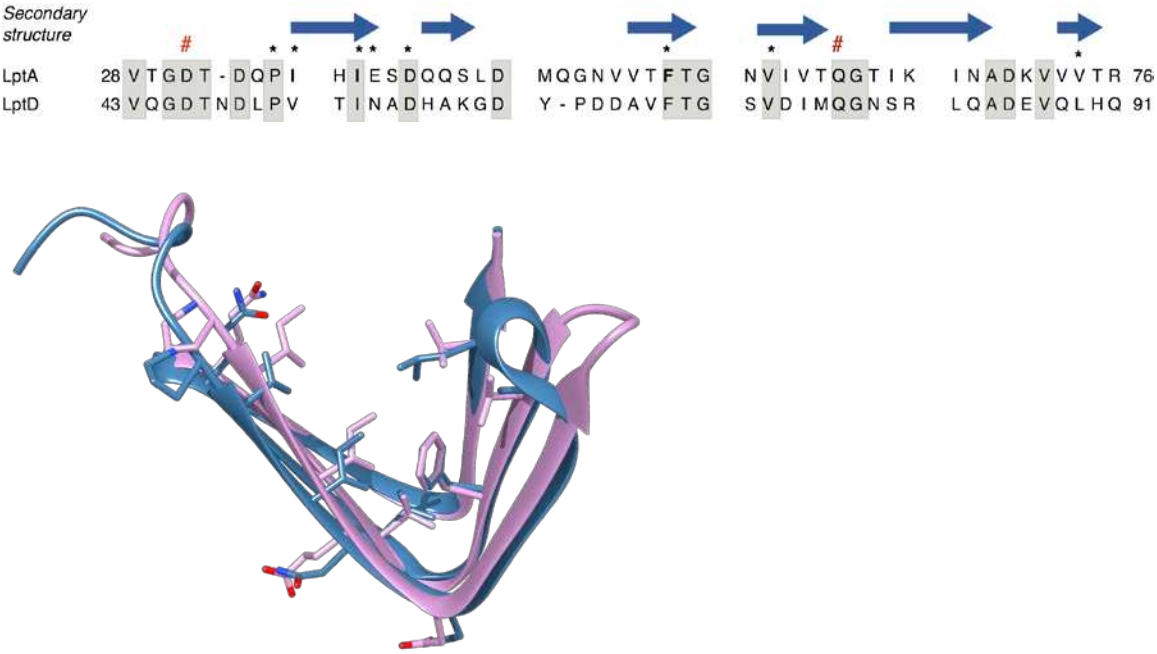

This close similarity between the N-terminal regions of LptA and LptD suggests that thanatin should bind to this region of LptD.

Table S7. Statistics from the NMR structure calculations for $LptA_m$-thanatin.

Input data for structure calculation	
NOE distance restraints	
total	1085
Intra-residue, i-j=0	285
Sequential, i-j=1	334
Medium-range, 1<i-j<5	62
Long-range, i-j ≥ 5	404
Torsion angle constraints	202
Structure statistics, 20 conformers	
CYANA target function value ($Å^2$)	1.7
Energies (kcal/mol)	
Total	-4305 ± 168
Distance restraints	32 ± 5
Satisfaction of Experimental Constraints:	
NOE distance restraints	
Max Violations per structure	0.30 ± 0.02
RMSD of violations	0.01 ± 0.00
Torsion angle restraints	
Max Violations per structure	11.5 ± 1.40
RMSD of violations	1.33 ± 0.15
PROCHECK Ramachandran plot analysis	
Residues in favored regions (%)	76.9
Residues in additional allowed regions (%)	22.9
Residues in generously allowed regions (%)	0.1
Residues in disallowed regions (%)	0.2
Root mean square deviation to the average coordinates (Å)	
Backbone atoms (residues 30-143,4-20)	1.33 ± 0.32
Backbone atoms (regular secondary structure)[a]	0.85 ± 0.22
Heavy atoms (residues 30-143, 4-20)	1.85 ± 0.31
Heavy atoms (regular secondary structure)[a]	1.31 ± 0.20

[a] residues 31-45, 51-75, 85-97, 106-115,123-130,135-141 and thanatin 4-20